DEVELOPMENT OF THE MECHANICAL DESIGN FOR A FREEZE-OUT PURIFIER

By

Duncan Kroll

A THESIS

Submitted to
Michigan State University
in partial fulfillment of the requirements
for the degree of

Mechanical Engineering – Master of Science

2020

ABSTRACT

DEVELOPMENT OF THE MECHANICAL DESIGN FOR A FREEZE-OUT PURIFIER

By

Duncan Kroll

Purification systems are necessary to support commissioning and operation of helium refrigeration and associated experimental systems. These systems are typically designed for a low level of impurity (i.e., in parts per million), since a 4.5 K or 2 K helium system will solidify, or freeze out, every other substance. The trace impurities can block and/or change the flow distribution in heat exchangers and potentially damage turbines or cryogenic compressors operating at high speeds. Experimental systems, such as superconducting magnets, require helium purification due to inherent characteristics in their construction. These are also used for the commissioning of sub-systems, like the compressors, and cold boxes. As known from experience, molecular sieves do not remove low-level moisture impurity sufficiently. Typical commercial freeze-out purifiers using molecular sieves have very short operating times between regenerations and are inefficient, requiring substantial utilities like liquid nitrogen and high-pressure operation. Based upon proven experience from a freeze-out purifier design for Brookhaven National Lab (BNL) in 1983, a liquid nitrogen assisted freeze-out purifier has been designed. This design includes a multi-pass and multi-stream heat exchanger and an activated carbon bed. The heat exchanger design is expected to minimize the liquid nitrogen usage and extend the capacity and the operating pressure range, thereby the time interval between regeneration. The goal is to provide a simple, naturally balanced design procedure to develop and operate an efficient purifier system.

ACKNOWLEDGEMENTS

First, I would like to express my sincere gratitude to my primary advisor, Dr. Abraham Engeda, for his support of my graduate studies. He initially connected me with FRIB, where I was able to do interesting and meaningful research. He continues to encourage me to aspire to greater achievements.

Dr. Pete Knudsen, Dr. Rao Ganni, and Dr. Nusair Hasan have extensive experience in cryogenics, and I am lucky to be able to draw from their wealth of knowledge on this subject. Their constant support of my project and availability to me when I have questions has been crucial to my success. Their ability to see the big picture when I had been focusing on the minutia of specific components was very helpful. Their work on the initial process study for this project was what allowed me to do this work in the first place. Dr. Hasan worked very closely with me throughout the design and writing of this thesis. I am very grateful for their guidance.

I would also like to thank Dr. Rebecca Anthony, along with Dr. Engeda, Dr. Knudsen, and Dr. Hasan for agreeing to be a part of my thesis committee.

Further thanks goes out to my coworkers. First, Adam Fila's work in modeling, designing, and building this helium purifier with me. I have learned a lot building the purifier and its prototype with him. Mat Wright assisted in my initial understanding of the existing FRIB purification system. His previous work in helium purification provided a useful guide to base my work on. My fellow graduate students Jon Howard and Tasha Williams were helpful in reviewing my work and providing a peer support system. Special thanks to Fabio Casagrande (Cryogenic Department Manager, FRIB), Thomas Glasmacher (Laboratory Director, FRIB), and the Accelerator Science and Engineering Traineeship program for providing me with the opportunity to work at FRIB.

Finally, I would like to thank my family. My parents, Kevin and Suzanne, and my sister, Sydney, have been very supportive throughout my education and have always pushed me to be the best I can, believing I will achieve it at every stage.

This material is based upon work supported by the U.S. Department of Energy Office of Science under Cooperative Agreement DE-SC0000661, the State of Michigan and Michigan State University. Michigan State University designs and establishes FRIB as a DOE Office of Science National User Facility in support of the mission of the Office of Nuclear Physics.

TABLE OF CONTENTS

LIST OF TABLES	vi
LIST OF FIGURES	viii
CHAPTER 1: INTRODUCTION	1
1.1 Background	1
1.2 Motivation	2
1.3 Project Description	2
CHAPTER 2: PROCESS DESIGN	3
2.1 Heat Exchanger	4
2.2 Nitrogen Boiler	7
2.3 Carbon Bed	8
CHAPTER 3: MECHANICAL DESIGN	11
3.1 Design Considerations	12
3.2 Mechanical Design of Heat Exchanger	14
3.3 Mechanical Design of Nitrogen Boiler	19
3.4 Mechanical Design of Carbon Bed	21
3.5 Mechanical Design of Process Piping	24
3.6 Mechanical Design of Insulating Vacuum Jacket	25
3.7 Selection of Miscellaneous Components	26
CHAPTER 4: FABRICATION PROCESS	27
4.1 Fabrication Considerations	27
4.2 Fabrication Plan	27
4.3 Fabrication of Prototype	30
CHAPTER 5: Modes of Operation	33
5.1 Modes of Operation	33
5.2 Description of Operating and Maintenance Procedures	34
5.3 Valve Position Matrix	49
CHAPTER 6: SUMMARY AND CONCLUSION	50
APPENDICES	51
APPENDIX A: STRESS ANALYSIS	52
APPENDIX B: PROCESS CALCULATIONS	66
APPENDIX C: MECHANICAL CALCULATIONS	67
BIBLIOGRAPHY	71

LIST OF TABLES

Table 2.1: Design requirements for the freeze-out purification system	4
Table 2.2: Constants for Equation 2.2	8
Table 3.1: Basic dimensions of the major components of the purifier	12
Table 3.2: Design parameters of the purifier	13
Table A.1: CAEPIPE B31.3 code compliance for nitrogen piping from nitrogen boiler to heat exchanger	53
Table A.2: CAEPIPE B31.3 code compliance for helium piping from supply to the heat exchanger	55
Table A.3: CAEPIPE B31.3 code compliance for helium piping from the heat exchanger to the nitrogen boiler	57
Table A.4: CAEPIPE B31.3 code compliance for helium piping from the nitrogen boiler to the carbon bed	59
Table A.5: CAEPIPE B31.3 code compliance for helium piping from the carbon bed to the heat exchanger	61
Table A.6: CAEPIPE B31.3 code compliance for helium piping from the heat exchanger to the recovery system	63
Table A.7: Analysis of maximum stress results	65
Table B.1: Carbon bed sizing calculations	66
Table C.1: B31.3 piping pressure design	67
Table C.2: BPVC internal pressure design	67
Table C.3: BPVC external pressure design	67
Table C.4: HX-1 mandrel vertical rod supports	68
Table C.5: Reinforced nozzle opening in carbon bed top head	69
Table C.6: Carbon bed screen supports	70
Table C.7: Component weight	70

 Table C.8: Component cool-down enthalpy

LIST OF FIGURES

Figure 2.1: Simplified flow diagram of the freeze-out purification system	3
Figure 2.2: Solid-liquid (S-L) saturation temperature of moisture as function of the mole fraction at different stream (operating) pressures [7]	6
Figure 2.3: Heat exchanger cooling curves for HX-1 (left) and HX-2 (right)	6
Figure 2.4: Effect of stream operating pressure on purifier operating period at maximum design contamination (moisture)	7
Figure 2.5: Adsorption curve for nitrogen on PCB carbon in terms of liquid nitrogen	9
Figure 3.1: Sketches showing (a) complete purifier assembly, (b) nitrogen boiler, (c) freeze-out heat exchanger (without outermost shell) and (d) carbon bed	11
Figure 3.2: Example of u-bend to limit thermal stress	13
Figure 3.3: Finned tubes being measured on reception	14
Figure 3.4: Cross-section of the heat exchanger	15
Figure 3.5: Rods supporting HX-1 mandrel for external pressure design	18
Figure 3.6: Example head analyzed using Ansys	18
Figure 3.7: FEA stress distribution of heads in heat exchanger	19
Figure 3.8: Detailed cross-sectional view of the nitrogen boiler assembly	20
Figure 3.9: Helium tubing coils in the nitrogen boiler	20
Figure 3.10: Left shows top header, right shows bottom header of helium coil	20
Figure 3.11: Detailed cross-sectional view of the carbon adsorber bed assembly	21
Figure 3.12: Stainless steel screen and associated components	22
Figure 3.13: 'Mott' filter assembly	23
Figure 3.14: Band heater model	23
Figure 3.15: View of purifier piping	24

Figure 3.16: Purifier head and connections	25
Figure 4.1: Fabrication plan step showing weld	28
Figure 4.2: Model of two sections of shell installed separately (arrows point to welds for this part)	29
Figure 4.3: Coiled tubes carefully spaced out on the mandrel	30
Figure 4.4: Tubes tied together with wires and cinched down with sheets and clamps	31
Figure 4.5: Heat exchanger with shell installed	32
Figure 5.1: Regular Operation P&I	36
Figure 5.2: Helium Blow Down P&I	38
Figure 5.3: LN2 Evaporation and Warm Up P&I	40
Figure 5.4: Heating P&I	42
Figure 5.5: Pump P&I	44
Figure 5.6: Backfill P&I	46
Figure 5.7: Cool Down and Purge P&I	48
Figure 5.8: Valve position matrix	49
Figure A.1: CAEPIPE model of nitrogen piping from nitrogen boiler to heat exchanger	52
Figure A.2: Stress distribution for helium piping from supply to the heat exchanger	54
Figure A.3: Stress distribution for helium piping from the heat exchanger to the nitrogen boiler	56
Figure A.4: Stress distribution for helium piping from the nitrogen boiler to the carbon bed	58
Figure A.5: Stress distribution for helium piping from the carbon bed to the heat exchanger	60
Figure A.6: Stress distribution for helium piping from the heat exchanger to the recovery system	62
Figure A 7. Stress distribution of heat exchanger headers/rings	64

CHAPTER 1: INTRODUCTION

1.1 Background

Helium has a wide range of applications in various scientific, space, medical and process industries. These industries take advantage of the very low (cryogenic) boiling temperature and chemically inert nature of helium. The known helium reserves are depleting, and this is reflected in the recent price escalations. Hence, not only from a technical aspect, but an economic one is there a need for helium purification and/or recirculation to minimize waste. In 2015, more than one-third of the total helium consumption in US was in the cryogenic refrigeration sector [1]. Cryogenic refrigerators which utilize helium as a refrigerant are necessary for systems using superconducting devices, such as magnetic resonance imaging and particle accelerators. These refrigeration systems operate at 4.5 K (the just above normal boiling point of helium), down to 1.8 K (which requires helium with vapor pressure of 16 mbar). At these very low temperatures, the presence of any other substances (contaminants) except helium will result in solidification. This can lead to damage to moving parts of the cryogenic system and/or affect the flow distribution in heat exchangers and flow blockage in valves. Obviously, these can have a deleterious effect on the refrigerator capacity and operations. Although usually better than industrial Grade-A (also Grade 4.7) purity helium is used in these refrigerators, contaminants are inadvertently introduced to the system through residuals leftover from a clean-up, air in-leaks to systems operating below 4.5 K, and out-gassing from cooled devices (e.g., magnets). The constituents from the first two are of oxygen, nitrogen and moisture. After the initial clean-up, these constituents are present in relatively low concentrations, of the order of 10 ppm or less. Although, this seems small, it can (and does) build up over time and consequently pose threat to the reliable and efficient operation of the equipment.

1.2 Motivation

From operational experience at Jefferson Lab and the Spallation Neutron Source [2], it was found that the molecular sieve is unable to remove low level moisture sufficiently, despite reasonable regeneration practices. This was evident from the pressure build-up in the helium-helium-nitrogen heat exchanger used to cool the helium to liquid nitrogen temperatures. To address these issues, several different methods of low level impurity removal [3-5] have been investigated in the past, including freeze-out (or refrigeration) purification [4]. For the latter, a heat exchanger specifically designed to accommodate the solidified moisture from a contaminated helium stream is used, rather than molecular sieve. This is a very effective method for removing low level moisture contamination due to the very low saturation vapor pressures. However, it requires a heat exchanger design that is well suited for contaminate solidification distribution and minimal impact on flow distribution. Typical commercially available freeze-out purifiers have a much shorter operating time in between regenerations and are not optimized for low pressure operation or efficient LN usage [6]. As such, there is a need for fundamental improvements of this critical subsystem.

1.3 Project Description

The development of a helium purification system utilizing freeze-out purifier heat exchanger is reported. The purification system is designed to remove low level impurities (mainly air), typically present in systems using superconducting devices at or below 4.5 K. The goal is to provide a simple design procedure to develop an energy/utility efficient helium purifier with a long operating interval between regenerations. This purifier will serve as the primary helium purification system for MSU-FRIB cryogenic refrigerator and superconducting magnet testing facility.

CHAPTER 2: PROCESS DESIGN

The helium purification process in the freeze-out purifier begins with the contaminated helium cooled to approximately 80 K in a counter-flow helium-helium-nitrogen heat exchanger (HX-1 and HX-2 in figure 2.1). Any moisture in the contaminated helium stream is solidified on the HX-1 surface. The contaminated helium is then cooled to at or below 80 K in a liquid nitrogen (LN) boiler, after which it flows through an activated carbon bed (also maintained at 80 K) where the remaining contaminants (like oxygen and nitrogen) are removed. Pure helium leaves the carbon bed, and its enthalpy is recovered in the counter flow heat exchangers (HX-2, then HX-1), exiting near ambient conditions from HX-1. Design goals for the freeze-out purification system are listed in table 2.1.

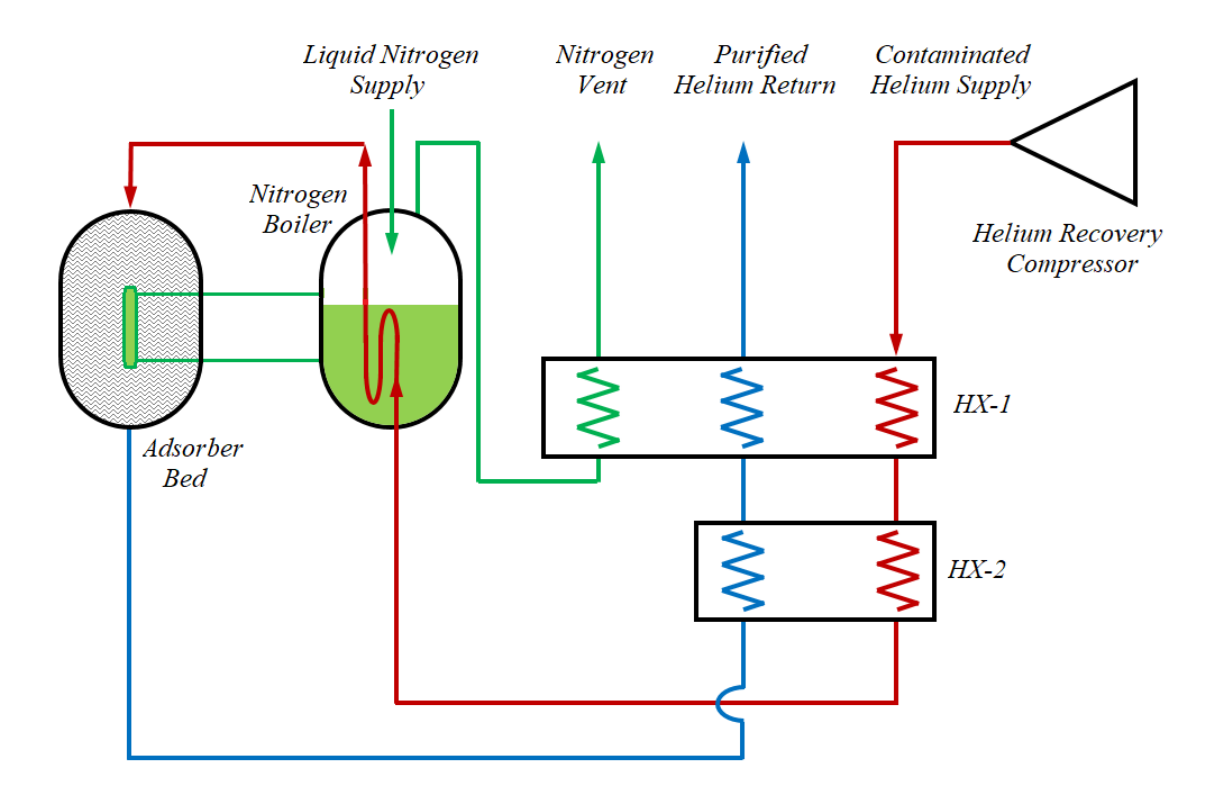


Figure 2.1: Simplified flow diagram of the freeze-out purification system

Table 2.1: Design requirements for the freeze-out purification system

Mass flow rate (helium)	30 g/s
Operating pressure	6.0 to 16.0 bar (helium)
Design pressure	18.0 bar (helium), 5.0 bar (nitrogen)
Design max. pressure drop	0.25 bar (tube side / shell side)
Design. max. contamination	30 ppm _v water, 30 ppm _v nitrogen
Minimum time between regenerations	14 days
Design LN usage	$0.05 \text{ m}^3/\text{hr}$

2.1 Heat exchanger

The heat exchanger is a major and critical component of the freeze-out purification system. Its effectiveness plays an important role in the purification capacity and LN consumption of the system. The type of heat exchanger is paramount to achieving the desired design requirements in a cost-effective manner. For this application, a coiled fin-tube heat exchanger type was selected. They is somewhat similar to those used in the small-scale refrigerators, and also known as Collins heat exchangers. The model for this heat exchanger was developed following the work reported by Yuksek [7], studied for the Linde 1600 helium refrigerator. This type of heat exchanger is comprised of one or several tubes wrapped fin-to-fin, in a helix around a mandrel, and enclosed by an outer shell. There can be one or multiple passes that are arranged in one or multiple wraps ('layers'). Multiple passes allow for higher volume (mass) flow, at a lower pressure drop and thus supporting low pressure operation to reduce compressor power. However, these multiple passes increase the heat exchanger mechanical design and fabrication complexity.

The contaminated helium flows in the annular space in-between and over the finned-tubes in a locally cross-flow manner (although the heat exchanger is overall in a counter-flow configuration). This design inherently has the characteristics for high contamination holding capacity with lower impact on the heat exchanger performance, like an increase in pressure drop or a reduction in effectiveness. The purified helium stream flows through the tubes which are wound about a mandrel and bounded by the outer shell. For this design six parallel passes of coiled fin-tubes (12.7 mm outside diameter tube, 4.8 mm fin height and 0.5 mm fin thickness) are used. For geometrical compactness and segregation of the trapped contamination (moisture), the heat exchanger is physically split into two sections (HX-1 and HX-2 referring to figure 2.1). HX-1 is designed for freeze-out entrapment of the moisture from the contaminated stream. Figure 2.2 shows the calculated solid-liquid (S-L) saturation temperature of moisture at the stated (total) pressure. The S-L saturation temperature of moisture is calculated using Raoult's law of partial pressures and polynomial fits to measured saturation temperatures obtained from [8]. It is observed that the S-L saturation temperature varies between 200 K and 240 K over the range of operating pressures. As such, HX-1 is designed to cool the contaminated stream from 300 K to 180 K. In this way, the trapped moisture stays in this section which facilitates the regeneration. An additional coiled fin-tubing is used in this heat exchanger section to recover the refrigeration from the nitrogen vapor stream (exiting the nitrogen boiler). HX-2 is designed to cool the contaminated stream from 180 K to 80 K, recovering the exergetically more valuable the refrigeration from the purified helium stream. The calculated cooling curves for both of these heat exchangers are shown in figure 2.3. From the HX-1 cooling curve, it can be estimated that approximately 25% of HX-1 axial length (as indicated by the percent total NTU's) is required to reduce (i.e., solidify) the contaminated stream moisture content from the design maximum of 30 ppm to 0.3 ppm (i.e. 1%

of the initial value). The heat transfer surface area corresponding to this length is approximately 6.5 m^2 .

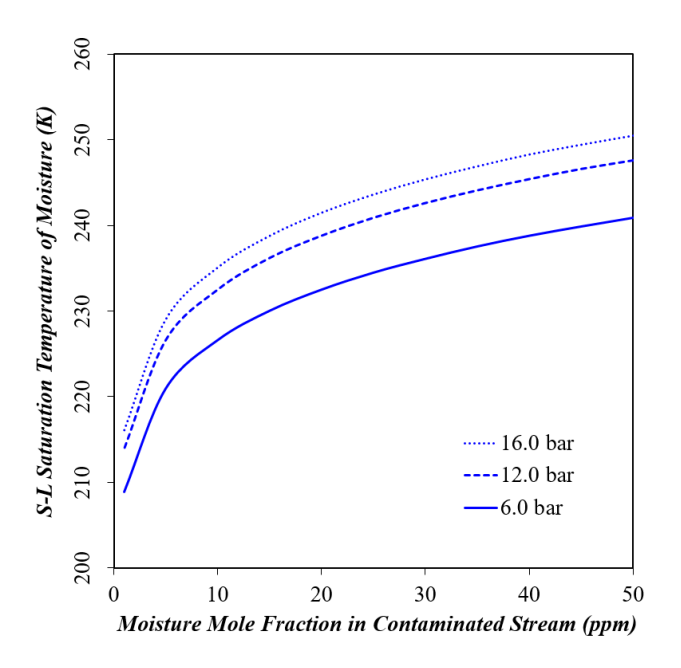


Figure 2.2: Solid-liquid (S-L) saturation temperature of moisture as function of the mole fraction at different stream (operating) pressures [7]

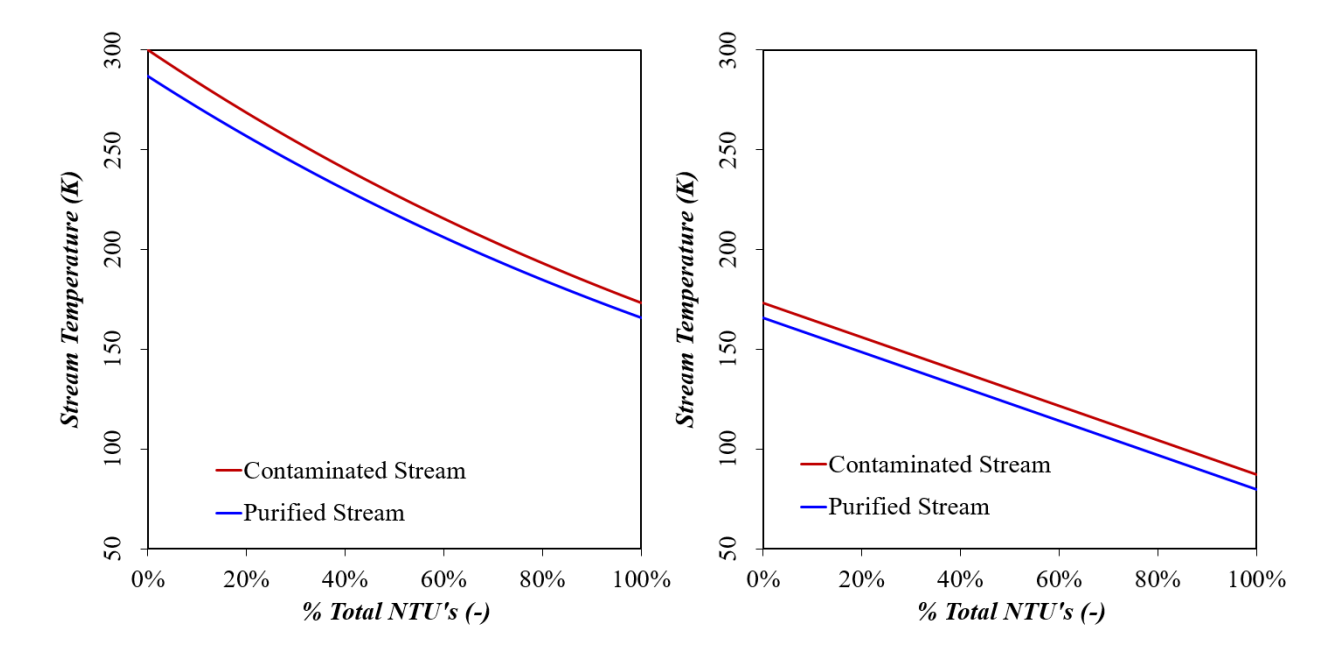


Figure 2.3: Heat exchanger cooling curves for HX-1 (left) and HX-2 (right)

Based on a design goal of maximum pressure drop of 0.25 bar and the surface area available to capture the moisture, it is estimated that up to 2.5 kg of moisture can be captured by HX-1. A parametric study on the effect of the operating pressure on the purifier operating time was performed and the results are shown in figure 2.4. From this figure, it is observed that with a moisture concentration of 30 ppm (at 30 g/s), the operating period of the purifier (*i.e.* time before HX-1 reaches a pressure drop of 0.25 bar) is about 30 days or longer.

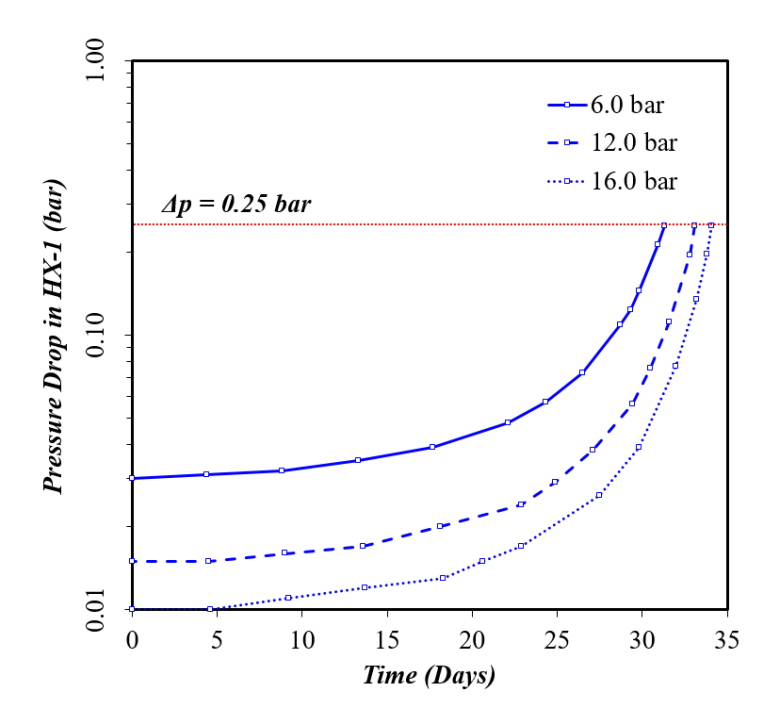


Figure 2.4. Effect of stream operating pressure on purifier operating period at maximum design contamination (moisture)

2.2 Nitrogen Boiler

The nitrogen boiler is the next major component of the purification system. The design of this component was performed following Wright, et al [9]. Based on an estimated LN consumption

of 0.05 m³/hr., a 0.17 m outside diameter (OD) vessel (approx. 0.05 m³ volume) was selected for the nitrogen boiler.

2.3 Carbon Bed

Activated carbon at 80 K is proven to be and effective media for adsorbing oxygen and nitrogen – the major species making up the contaminant. The carbon bed was sized based on the volume of carbon required. This was determined from the design parameters for mass flow rate of helium, desired break through time, and pressure drop. Two methods were used to find the specific adsorbent capacity of the carbon. The first calculates the excess adsorption energy, $(\varepsilon_{ij})_{eq}$ (in cal/mol) using the following equation:

$$(\varepsilon_{ij})_{eq} = RTln(P_s/p)$$
 Equation 2.1

Here, R is the specific gas constant (nitrogen), T is the operating temperature, P_s is the saturation pressure of nitrogen at 80 K, and p is the partial pressure of nitrogen. Then equation 2.2 is used. It is derived from figure 2.5 to find the nitrogen adsorbed (in cm³liq/100g activated carbon).

$$N_2$$
 adsorbed = $Av^5 + Bv^4 + Cv^3 + Dv^2 + Ev + F$ Equation 2.2

Table 2.2: Constants for Equation 2.2

Constant	Value
A	-2.1720×10^{-18}
В	2.9064×10^{-14}
C	1.2939×10^{-10}
D	1.3893×10^{-7}
E	-2.7232x10 ⁻⁴
F	1.6802

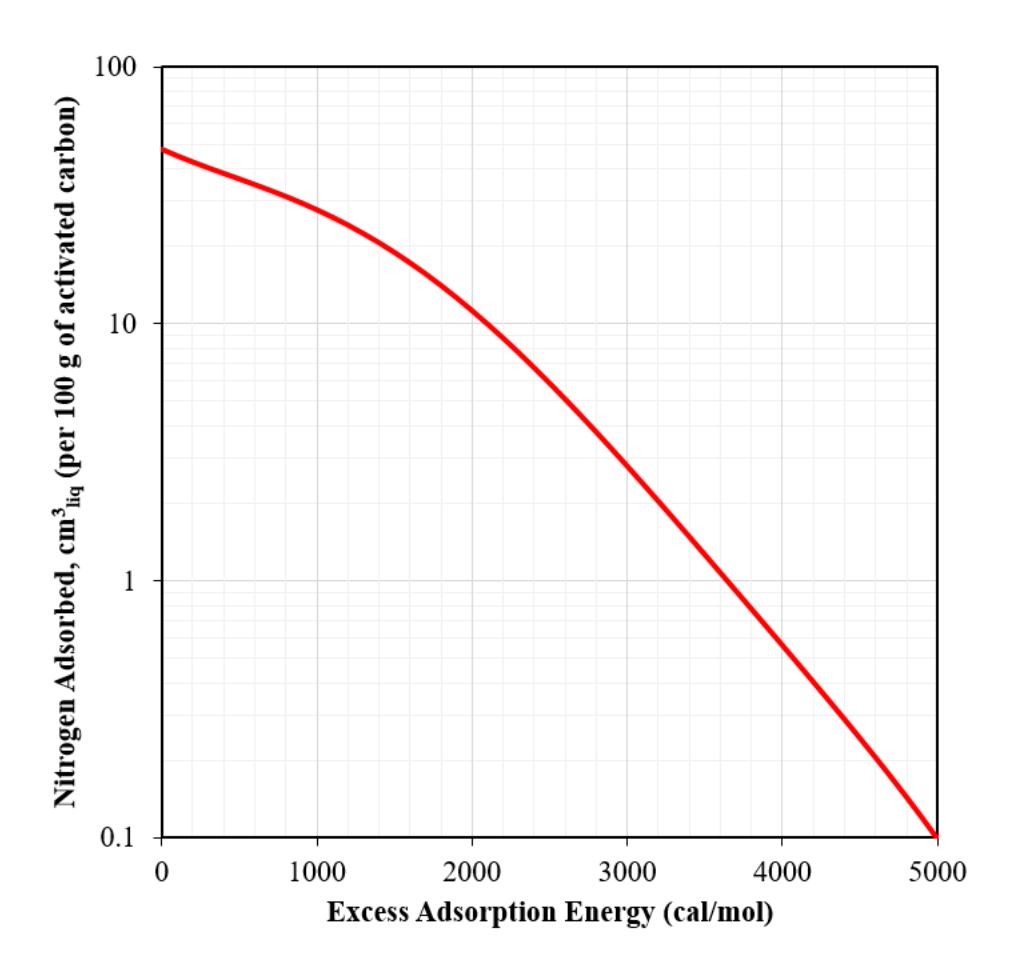


Figure 2.5: Adsorption curve for nitrogen on PCB carbon in terms of liquid nitrogen

The volume of carbon was calculated. This was based on a pre-determined bed diameter and a diameter to length ratio. A 12 NPS pipe was chosen for this because it would allow the purifier to be the desired size. A diameter to length ratio of 5 was chosen based on analysis done by Wright, et al. Once the volume was established, the breakthrough time, or time that the carbon takes to come to its adsorption capacity, was calculated using the following equation.

$$t_{BT} = \frac{V_C \rho_C * (N2 \ adsorbed)}{m_{N_2}}$$
 Equation 2.3

 V_C is the volume of carbon, ρ_C is the density of carbon, and m_{N2} is the maximum mass flow rate of nitrogen. The maximum flow rate of nitrogen was calculated using the maximum nitrogen

contamination of 30 ppm and the planned flow rate of helium of 30 g/s. The result was a break through time of approximately 22 days. This fits the goal of at least 14 days.

The pressure drop over the bed was also evaluated. The Ergun Equation (equation 2.3) was used.

$$\frac{\Delta P}{L} = \frac{150\mu G (1 - \varepsilon)^2}{kg\rho D^2} + \frac{1.75G^2 (1 - \varepsilon)}{kg\rho D\varepsilon^3}$$
 Equation 2.4

'ΔP' is pressure drop, 'L' is bed height, ' μ ' is fluid viscosity, 'G' is mass velocity, ' ϵ ' is inter-particle void fraction, 'k' is a conversion factor, ' ρ ' is fluid density, and 'D' is effective particle diameter. A pressure drop of 0.0708 psi was calculated. This is less than previous literature values of 0.1 psi, and below the 3 psi allowable limit. The results of these process calculations are found in Appendix B.

CHAPTER 3: MECHANICAL DESIGN

The purifier design has three major pressure vessels – a freeze-out heat exchanger, a nitrogen boiler, and an adsorber bed. All three pressure vessels operate at cryogenic temperatures and are enclosed in a vacuum insulating shell. The complete purifier assembly along with its major components are shown in figure 3.1 below.

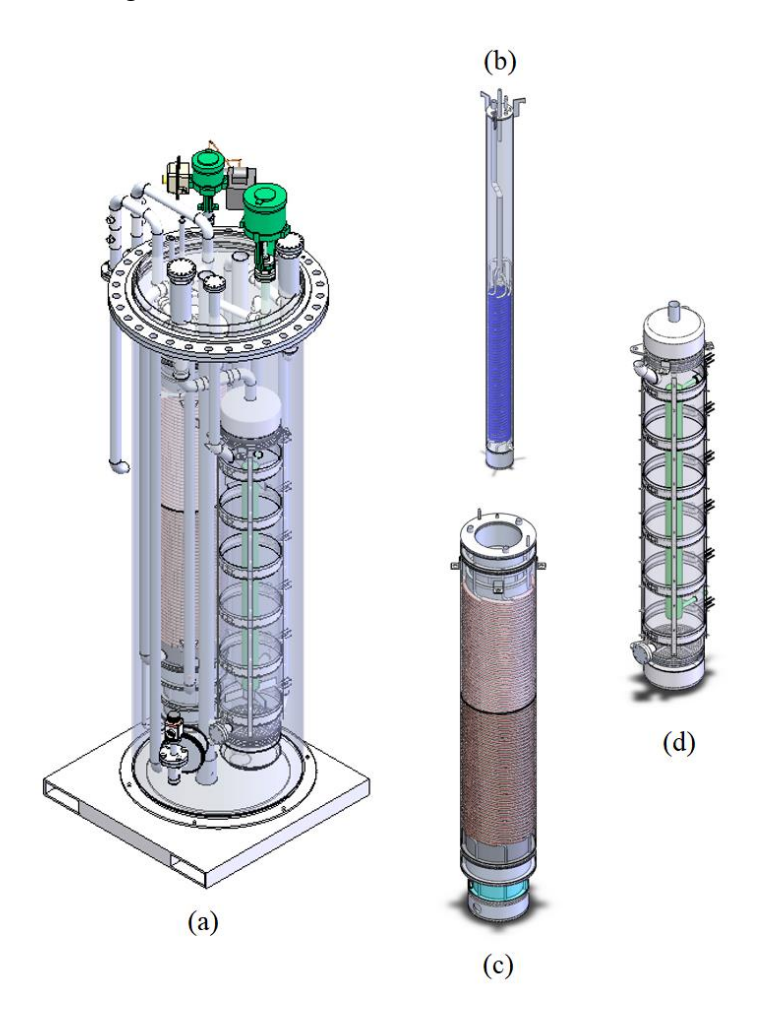


Figure 3.1: Sketches showing (a) complete purifier assembly, (b) nitrogen boiler, (c) freeze-out heat exchanger (without outermost shell) and (d) carbon bed

Mechanical design of the purifier piping and pressure vessels were performed following American Society of Mechanical Engineers (ASME) B31.3 Code and ASME Boiler and Pressure Vessel Code (BPVC), respectively. Piping flexibility analysis for the cryogenic process piping was performed for design in accordance with the ASME B31.3. Pressure design of different novel components were carried out using finite element analysis and following ASME B31.3 and BPVC (as applicable). Basic dimensions of the purifier are listed in table 3.1, and their design details are discussed in the following sub-sections.

Table 3.1: Basic dimensions of the major components of the purifier

Components	Outside Diameter	Shell Thickness	Nominal Length
	<i>(m)</i>	(mm)	(m)
Insulating vacuum shell	0.91	7.92	3.05
HX-1 Mandrel	0.27	6.35	2.15
HX-1 Shell	0.33	3.97	2.11
HX-2 Mandrel	0.36	7.92	1.83
HX-2 Shell	0.41	4.78	1.95
Nitrogen Boiler Shell	0.17	3.40	2.54
Carbon Bed Shell	0.33	4.57	2.03

3.1 Design Considerations

The materials used in the purifier were chosen based on their specific uses. ASTM A312 TP304L stainless steel was used for all the piping and vessels. This was chosen because it is an industry standard that will economically meet the requirements. ASTM SB75 C122 Copper was used for the finned tubes. The fins are ASTM SB75 C102 Copper. Copper conducts heat very well, allowing for very good heat transfer between process streams.

Table 3.2: Design parameters of the purifier

Design Pressure	18.0 bar (helium), 11.0 bar (nitrogen)
Design Temperature Range	80 K – 300 K

Thermal contraction and expansion was considered in this design. The thermal expansion coefficient of stainless steel (from 300 K to 80 K) is 17.3x10⁻⁶ m/m/K. There are several points where it could have caused stress. Thermal stress calculations were done. The only areas that failed stress tests were in the piping outside the process vessels. Piping loop were incorporated into the piping to reduce heat leak and stresses due to thermal contraction (at cryogenic temperatures), as well as for thermal stability. An example of this is shown in figure 3.2. The stress analysis of piping sections is shown in Appendix A.



Figure 3.2: Example of u-bend to limit thermal stress

3.2 Mechanical Design of Heat Exchanger

The heat exchanger is a major and critical component of the freeze-out purification system. Its effectiveness plays an important role in the purification capacity and LN consumption of the

system. The type of heat exchanger is paramount to achieving the desired design requirements in a cost-effective manner. For this application, the coiled fin-tube heat exchanger type was selected, which is somewhat similar to those used in the small-scale refrigerators, also known as a Collins heat exchanger. The finned tubes allow for a very large heat transfer surface area, while keeping the volume low. Figure 3.3 is a picture of the finned tubing used in this purifier.



Figure 3.3: Finned tubes being measured on reception

The model for this heat exchanger was developed following the work reported by Yuksek [7], studied for the Linde 1600 helium refrigerator. This type of heat exchanger is comprised of one or several tubes wrapped fin-to-fin, in a helix around a mandrel, and enclosed by an outer shell. There can be one or multiple passes that are arranged in one or multiple wraps ('layers'). Multiple passes allow for higher volume (mass) flow, at a lower pressure drop and thus supporting low pressure operation to reduce compressor power. However, these multiple passes increase the heat exchanger mechanical design and fabrication complexity. The heat exchanger is shown in figure 3.4 below.

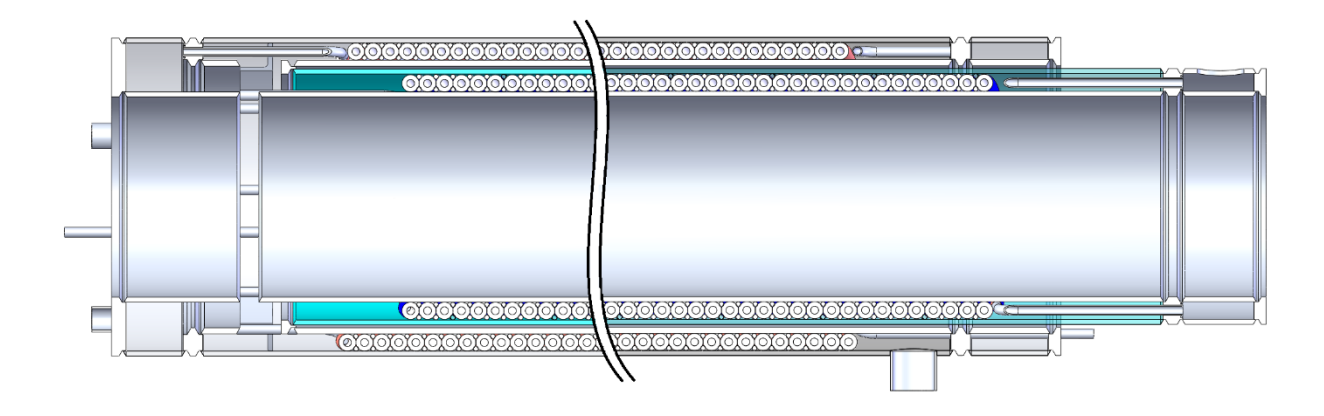


Figure 3.4: Cross-section of the heat exchanger

The contaminated helium flows in the annular space in-between and over the finned-tubes in a locally cross-flow manner. The heat exchanger is overall in a counter-flow configuration, as the flow globally goes up on one side and down on the other. This design inherently has the characteristics for high contamination holding capacity with lower impact on the heat exchanger performance. For geometrical compactness and segregation of the trapped contamination (moisture), the heat exchanger is physically split into two sections (HX-1 and HX-2 referring to figure 2.1). HX-1 is designed for freeze-out entrapment of the moisture from the contaminated stream. The purified helium stream flows through the tubes which are wound about a mandrel and bounded by the outer shell. For this design six parallel passes of coiled fin-tubes are used for HX-2, while seven are used for HX-1. This amounts to six helium passes in HX-2, with HX-1 having five helium passes and two nitrogen passes.

Annular flat heads at the ends of both heat exchangers serve as headers for tube and shell flows. At the top, the HX-1 tubes go through the heads and into a mixing chamber. The helium then goes back through the head into the HX-2 tubes. At the bottom the tubes go through the head, into the mixing chamber and exit through two inch pipes, or the reverse. The fin side flow comes in through two inch pipes which opens up to the fins. The helium flows up over the fins, then over

a ring connecting the mandrel of HX-1 and the shell of HX-2. It then goes out the same way it came in.

The mechanical design of the heat exchanger was done using ASME code standards, including B31.3 and BPVC. Internal pressure of shells was calculated using BPVC Section VIII-2, from the following equation:

$$P = \frac{SEt}{R + 0.6t}$$
 Equation 3.1

where P is design pressure, S is allowable stress for the material, E is the quality factor, t is vessel thickness, and R is inside radius. The results of this and all following calculations can be found in Appendix C.

External pressure of the shells was calculated using BPVC Section VIII-2 as well. It uses the length to diameter and diameter to thickness ratios on the charts in appendix to find the B value used in following equation:

$$P_a = \frac{4B}{3(D_o/t)}$$
 Equation 3.2

where P_a is the maximum pressure the vessel can withstand, B is an intermediate factor based on vessel size, and D_o is the outer diameter.

For the HX-1 mandrel, the external pressure required a thickness greater than desired for geometrical fit. Stiffening rings were considered to solve this. The allowable pressure when using stiffening rings was calculated using the same method as above, adjusting the effective length for the number of stiffening rings. The stiffening rings' moment of inertia was calculated using the BPVC equation:

$$I_s = \left[D_o^2 2L_s \left(t + \frac{A_s}{L_s}\right)A\right] / 14$$

where I_s is the moment of inertia, L_s is the effective length, A_s is the cross-sectional area of the stiffening rings, and A is an intermediate factor based on vessel size. This was compared with the available moment of inertia for the ring cross-section. From this comparison, the necessary size of stiffening ring was chosen.

Stiffening rings were found to be too bulky to fit in the small gap between the two heat exchangers, so another solution was pursued. This was using vertical tube supports at various points circumferentially between the shells. The calculation was done following *Roark's Formulas* for *Stress and Strain*, by Young and Budynas [10]. Table 15.2: Formulas for elastic stability of plates and shells details the calculation as shown below:

$$q' = \frac{E\frac{t}{r}}{1 + \frac{1}{2}(\frac{\pi r}{nl})^2} \left\{ \frac{1}{n^2 \left[1 + \left(\frac{nl}{\pi r}\right)^2 \right]^2} + \frac{n^2 t^2}{12r^2 (1 - v^2)} \left[1 + \left(\frac{\pi r}{nl}\right)^2 \right]^2 \right\}$$
 Equation 3.4

where q' is the critical pressure, E is the modulus of elasticity, t is the thickness of the shell, r is the outer radius of the shell, n is the number of supports, l is the length of the shell, and v is Poisson's ratio for the shell. The main input parameter is the number of supports. Four supports were found to be necessary to support the external pressure acting on the shell. A segment of the shells showing this design solution is in figure 3.5. The two shells in the figure are the HX-2 outer shell and the HX-1, with the rods in the vacuum space between the two heat exchangers.

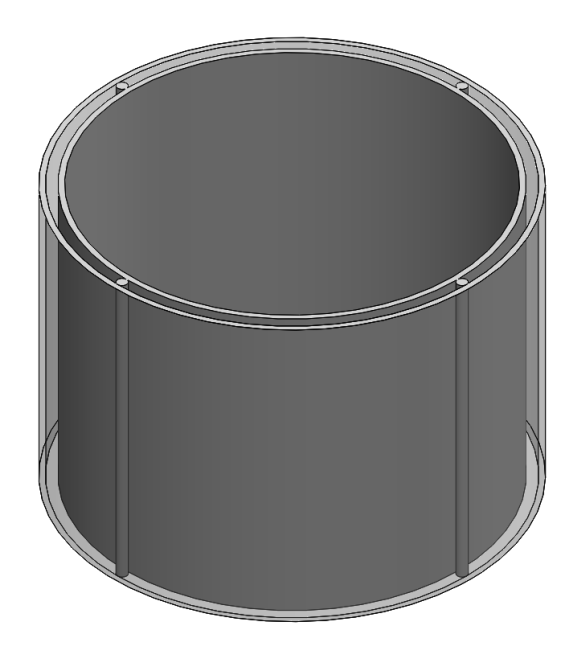


Figure 3.5: Rods supporting HX-1 mandrel for external pressure design

All of the heads (an example of which is shown below in figure 3.6) were analyzed using finite element analysis (FEA) in Ansys Workbench and compared to BPVC standards. These heads include boundaries between process streams, pressure boundaries, and structural supports.



Figure 3.6: Example head analyzed using Ansys

The boundary conditions used were test pressure, vacuum side pressure (17 psia), and supports (in this case fixed and cylindrical). The reported values were equivalent von-mises stress,

as requested in BPVC. These values were compared to the maximum allowable stress values given in ASME BPVC Section II for the material being used. The results of the analyses come in the form of a maximum stress and a stress distribution, the latter of which is shown below in figure 3.7 for all four types of heads in the heat exchanger.

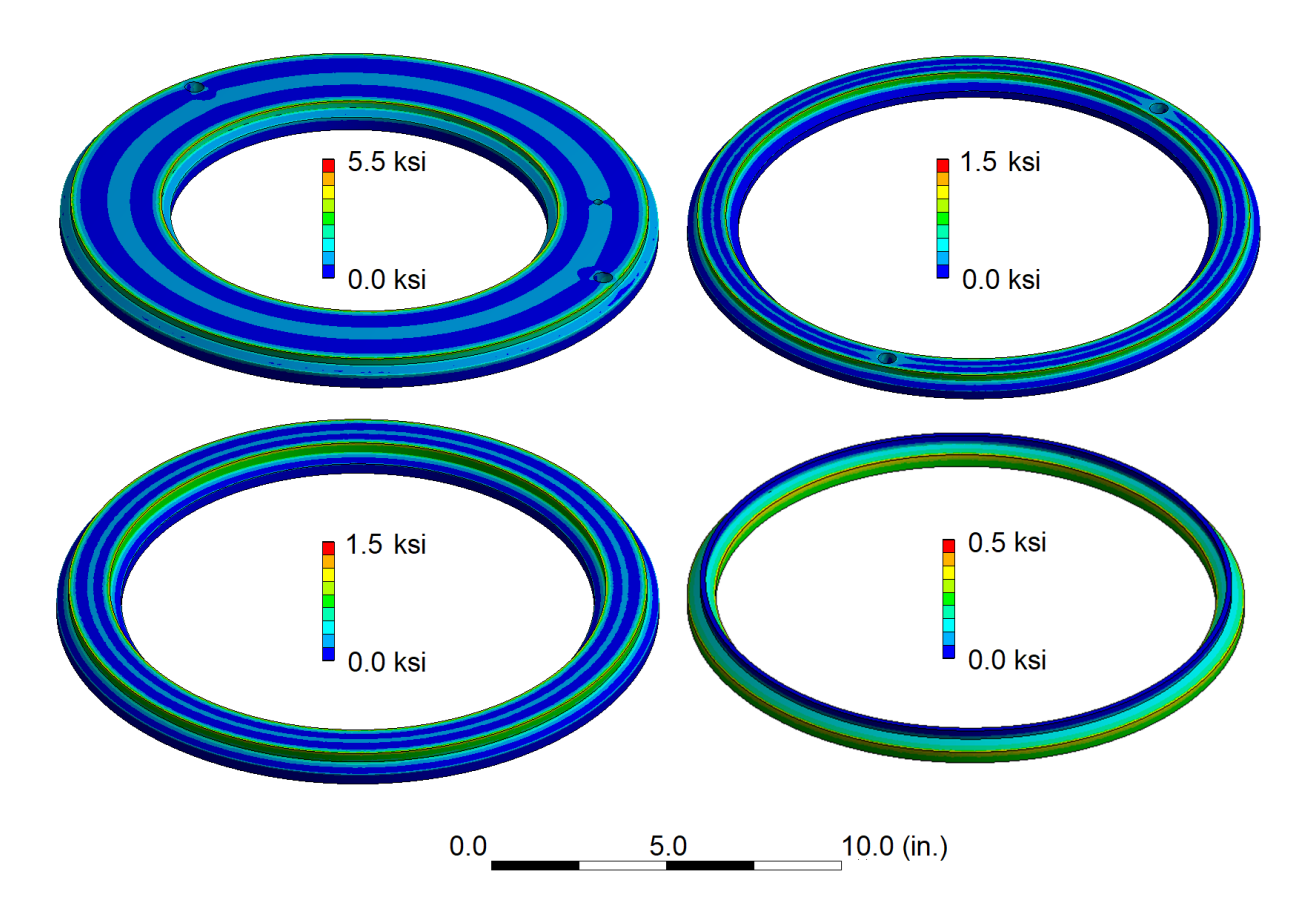


Figure 3.7: FEA stress distribution of heads in heat exchanger

3.3 Mechanical Design of Nitrogen Boiler

The nitrogen boiler consists of six parallel passes of stainless-steel tubing coiled inside a vessel, as shown in figure 3.8. Contaminated helium from the freeze-out heat exchanger (HX-2) outlet flows through the coiled tubing submerged in the liquid nitrogen and is then fed to the

adsorber bed. The nitrogen boiler is nested inside the annular vacuum space of HX-2 for compactness and minimizing radiation heat in-leak to the liquid nitrogen bath.



Figure 3.8: Detailed cross-sectional view of the nitrogen boiler assembly

The coil consists of six tubes. This coil is shown in figure 3.9. They begin by coming out of the bottom of the pipe that comes from the top. The flow recombines when the tubes go through a head at the bottom, as seen in figure 3.10.

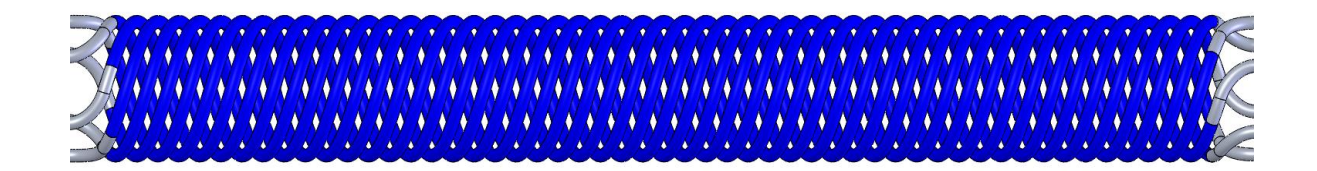


Figure 3.9: Helium tubing coils in the nitrogen boiler

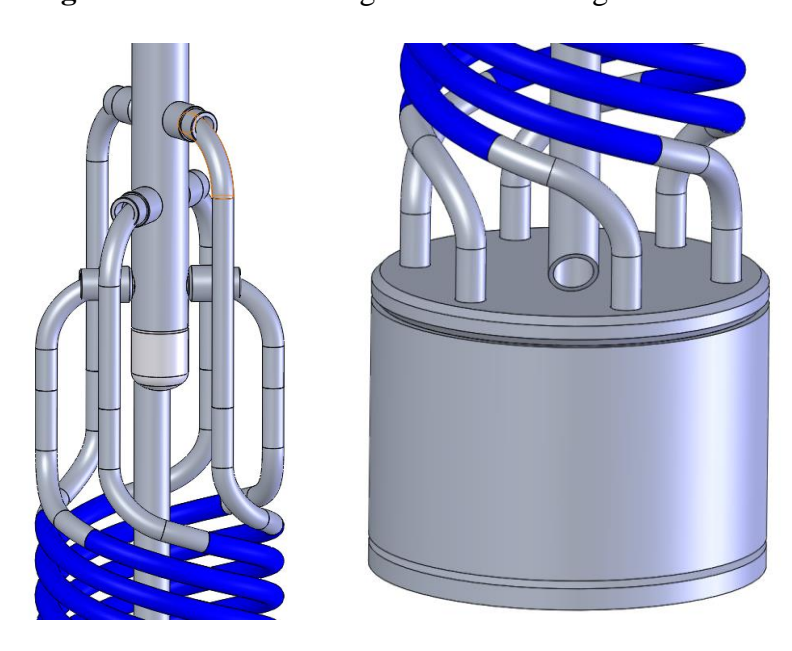


Figure 3.10: Left shows top header, right shows bottom header of helium coil

The boiler was much simpler to design than the heat exchanger. There was one pressure vessel, designed using the equations above for internal and external pressure at 5 bar. The heads were designed using Ansys Workbench, the same way the heat exchanger heads were designed.

3.4 Mechanical Design of Carbon Bed

The carbon bed is comprised of two pressure vessels, one nested inside the other. The outer vessel holds the adsorbent (activated carbon) in a fixed bed, while the inner vessel is mounted at the center of the fixed bed, supported by the inlet and outlet nitrogen piping. Liquid nitrogen flows through the inner vessel keeping the adsorbent at a constant temperature (approximately 80 K). The adsorbent is held in place within the fixed bed using layers of wire mesh screens and fiberglass filter. In addition, sintered metal filters are used at the inlet and outlet nozzles to the adsorber bed to prevent any carry-over dust from the exiting pure helium. Band heaters are mounted to the outer vessel shell for the regeneration process. A detailed cross-sectional view of the adsorber bed assembly is shown in figure 3.11.

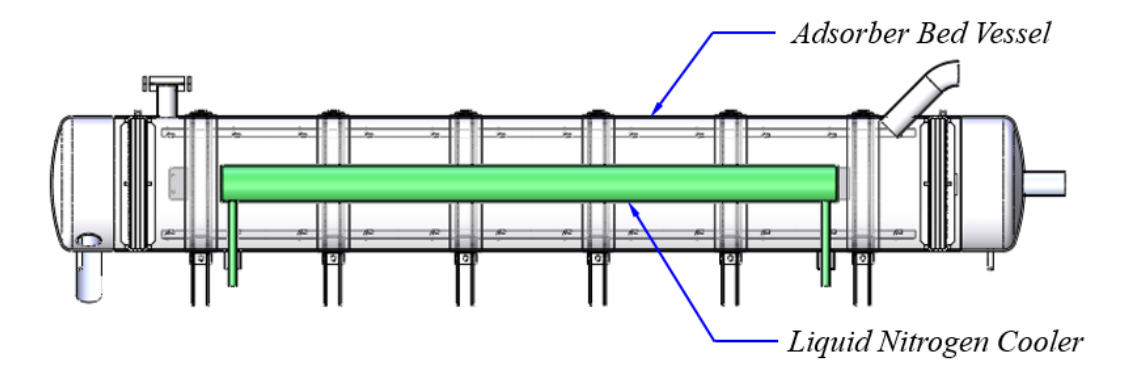


Figure 3.11: Detailed cross-sectional view of the carbon adsorber bed assembly

The two pressure vessels were designed as previously discussed. Wire mesh screens have been designed, with beam supports, to hold the weight of the carbon in the bed. Equation 3.5 shows

the calculation for designing the beam supports, which was done following *Roark's Formulas for Stress and Strain*, table 15.1:

$$W' = 1.67 \frac{2.82b^3 d \sqrt{\left(1 - 0.63 \frac{b}{d}\right) EG}}{l^2} \left[1 - \frac{1.74a}{l} \sqrt{\frac{E}{G\left(1 - 0.63 \frac{b}{d}\right)}} \right]$$
 Equation 3.5

where W' is critical load, b is horizontal width of the beam, d is vertical depth of the beam, E is the modulus of elasticity, G is the shear modulus, l is the length of the beam, and a is half of the vertical depth of the beam.

Stainless steel screens, as shown in figure 3.12, were used to preliminarily contain the carbon and keep it packed. Affixed to the top screen is a pipe section with another screen on top. The purpose of this screen is to divert some of the flow to the outside of the bed for an even flow distribution, so it uses the full radius of the carbon bed to adsorb impurities. This prevents the need for premature regeneration (before all the carbon is saturated) because the helium is only flowing over the center of the bed, saturating only the carbon in the center.

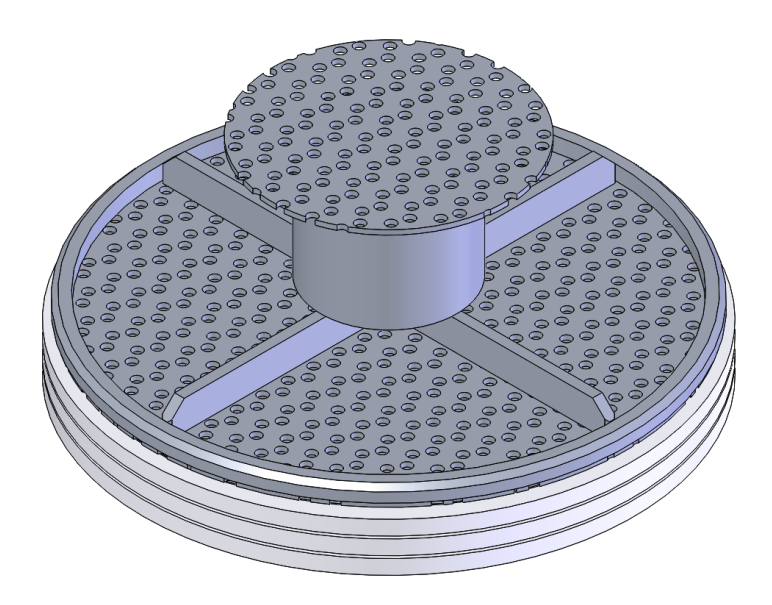


Figure 3.12: Stainless steel screen and associated components

'Mott' filters were used to make sure no carbon gets in the process stream outside of the adsorber bed. A model of the one used is shown below in figure 3.13.



Figure 3.13: 'Mott' filter assembly

Band heaters, as shown in figure 3.14, were wrapped around the bed to heat it above ambient temperature during regeneration. Six heaters were used, spaced 12.5 inches apart to assure equal heating through the bed.

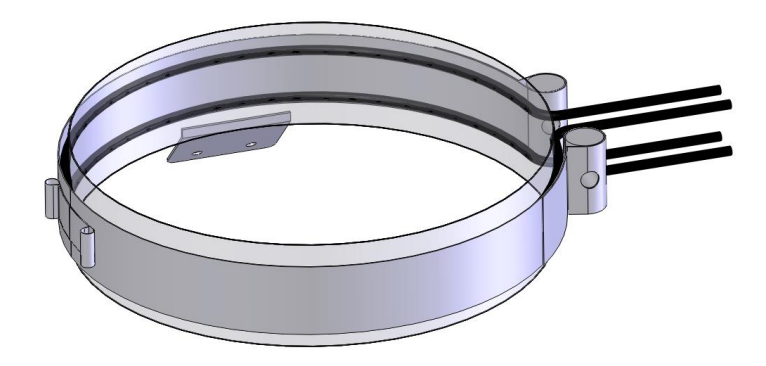


Figure 3.14: Band heater model

3.5 Mechanical Design of Process Piping

Piping design was done using ASME B31.3 Code. The following equation was used to calculate the necessary pipe thickness:

$$t = \frac{PD}{2(SEW + PY)}$$
 Equation 3.6

where 't' is required pipe thickness, 'P' is design pressure, 'D' is pipe outside diameter, 'S' is the allowable stress for the material, 'E' is a quality factor, 'W' is the weld joint strength reduction factor, and 'Y' is a coefficient based on temperature and material. This was done for every pipe in the purifier, including helium and nitrogen lines, and the nitrogen tank in the carbon bed. A portion of the purifier piping is shown in figure 3.15.

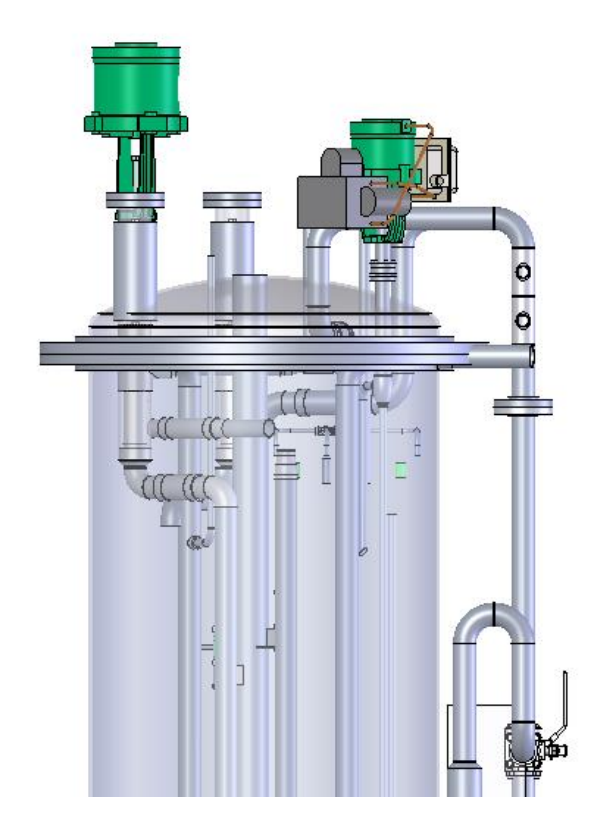


Figure 3.15: View of purifier piping

Flexibility analysis was done on the piping in Ansys. Thermal stresses were taken into account when this was done. The results of these calculations are shown in Appendix A.

3.6 Mechanical Design of Insulating Vacuum Jacket

The vacuum jacket for the purifier is a 36 NPS pipe with a standard ASME dished head. The vacuum shell was designed as a pressure vessel. All components inside the shell are mounted from this head. The insulating vacuum shell is attached to the head using a flanged connection, allowing access to the inner cryogenic components without cutting the vacuum shell. Cryogenic valves, instrumentation and maintenance ports are mounted to the top and side of the dished head. Figure 3.16 is a view of the head with all the connections.

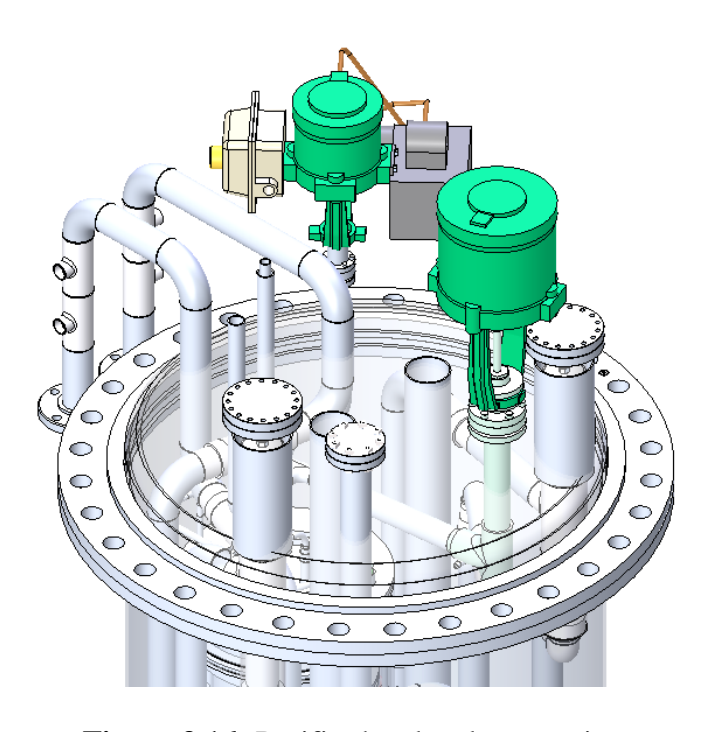


Figure 3.16: Purifier head and connections

3.7 Selection of Miscellaneous Components

All cryogenic components are wrapped with multi-layer insulation (MLI) to minimize radiation heat in-leak to the process. In addition, there is an external valve and instrumentation panel. All of the vales in the purifier are controlled from this rack. The design of this valve rack was optimized for ease of use. The valves are organized into rows and grouped by their main functions. For example, when in normal operation, only the top row of valves are open. This same pattern is seen in the instrumentation panel. This is further detailed in section 5.1: Modes of Operation.

A recirculation blower and an evaporator will be used for warm up of the purifier from the 300 K end circulating helium in the tube side, nitrogen boiler, and carbon bed. This circulation is further explained in section 5.1: Modes of Operation. Band heaters are mounted on the outside of the carbon bed for further warming above the ambient temperature. The nitrogen vessel in the carbon bed will assist the cool down following regeneration.

CHAPTER 4: FABRICATION PROCESS

4.1 Fabrication Considerations

There were many considerations taken into account when planning the fabrication of this purifier. The largest consideration was the small spaces available for welding. The order in which parts were assembled was crucial in solving these problems. There were some welds that were initially planned to be done near more heat-sensitive parts (namely the copper fins on the tubes). The method of assembly was changed to avoid welding near these parts. ASME welding standards disallowed some of the initially intended welds, because of the proximity of the welds to thin parts or other welds. The design of those parts was changed as necessary to allow for ASME-approved welds.

4.2 Fabrication Plan

A cross-sectional sketch of the heat exchanger was notated with the required welds in order of fabrication to show its viability. A sketch was drawn for each of the initial designs. The design that allowed for the easiest fabrication was chosen. A detailed, step-by-step fabrication plan was created from this sketch, showing a picture from the model of each of the 26 steps, including welds. This plan significantly helped the design process. It made some issues with the design more apparent. Some welds, like the one shown in figure 4.1, are very difficult to complete, or cause other problems [11]. The problem with this particular step is that the heat-effected zone of the weld between the two sections of shell includes the ropes underneath. This would cause the ropes to burn. The solution to this was to keep the shell in one piece, despite the larger amount of friction caused by the longer shell. The fabrication plan was then changed accordingly.

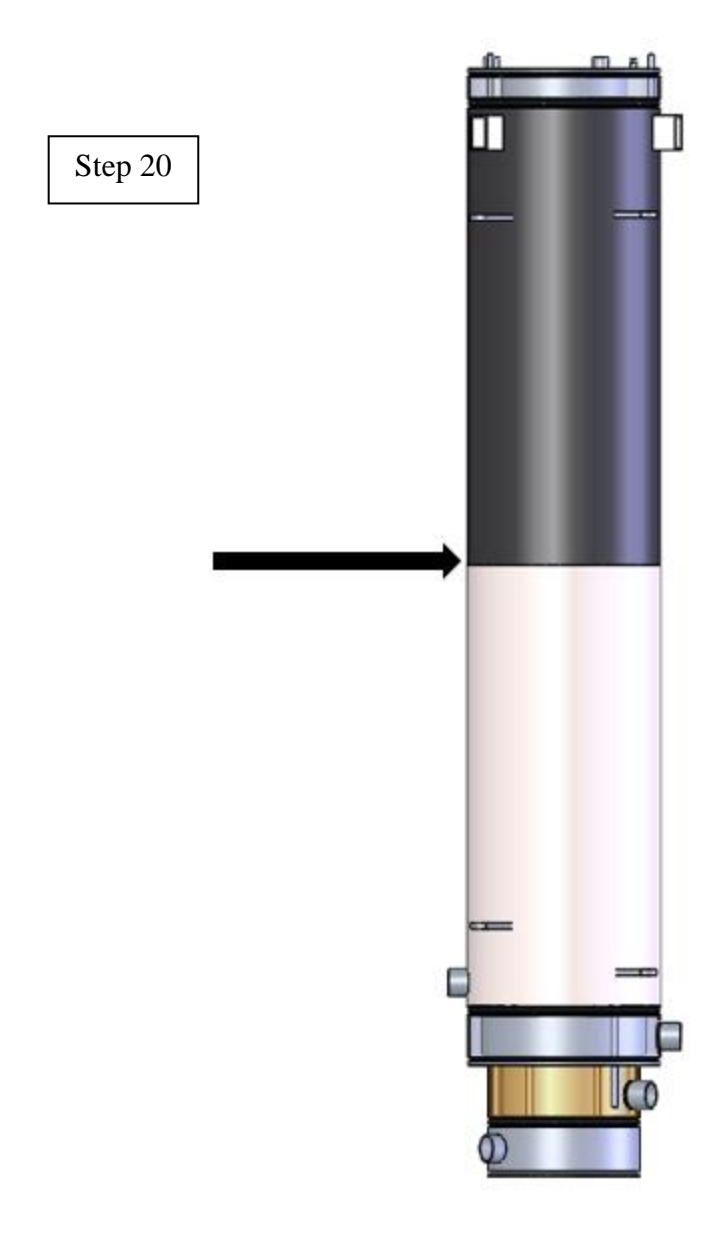


Figure 4.1: Fabrication plan step showing weld

Another area that needed to be reconsidered was the connection between the finned tubes and the rings that combine the flow into a mixing chamber. The copper finned tubes needed to be brazed to stainless steel tubes, which were then welded to the ring. It was difficult to guarantee the position of the ends of the finned tubes, so the stainless steel tubes needed to be field-fitted to assure a good fit. The space between the end of the copper tubes and the holes in the ring were

measured. Then, stainless steel tubes were cut and bent into shape. The stainless steel tubes were installed by pulling the copper tubes away from the mandrel and brazing them to the steel tubes, then feeding the steel end through the hole in the ring. The weld is the last step. This process underwent several iterations, including welding the ring to the mandrel at different times in the process, before this order was decided on.

Some small sections of shell need to be placed in between two rings that need (by ASME code) to be as wide as the shell. This means that the shell cannot be slid over the rings.

Therefore, either one ring has to be installed after the section of shell, or the shell needs to be installed in parts, so it doesn't need to slide over the rings. The latter solution was decided on to allow for easier fabrication of other parts of the heat exchanger. The bottom sections of shell, surrounding the mixing chambers between the rings, were chosen to be installed in two pieces, welded together in place. A model of this is shown in figure 4.2.

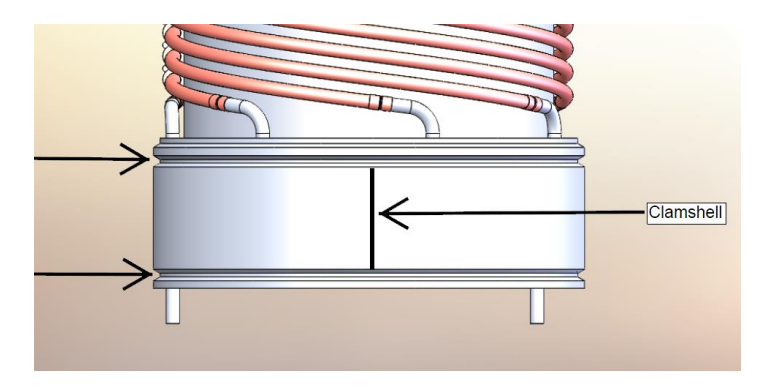


Figure 4.2: Model of two sections of shell installed separately (arrows point to welds for this part)

The rest of the purifier, including the carbon bed and nitrogen boiler, will be fabricated according to the design laid out in Wright, et al [9]. The changes made to that design are not significant enough to change the fabrication process.

4.3 Fabrication of Prototype

A prototype of HX-2 was built and tested to find and solve the issues that came up with the fabrication. This was done during the design process, so many of the parts were not their final size. The largest difficulty encountered during the fabrication of the prototype was tightening the coils of finned tubes together and to the mandrel. The coils needed to be tightened so there was no space between them. This was to prevent any gas bypassing the fins. They had significant friction between each other because of the fins, making this difficult. The coils had to be pulled apart slightly in order for them to be moved. This spreading of the some of the coils is shown in figure 4.3. The first three coiled tubes are spread apart, so the next three can be placed in the gap. Here, small metal sheets are being used to keep the fins from interlocking and stopping the movement of the tubes. In the figure, the second three tubes are partially screwed into place.

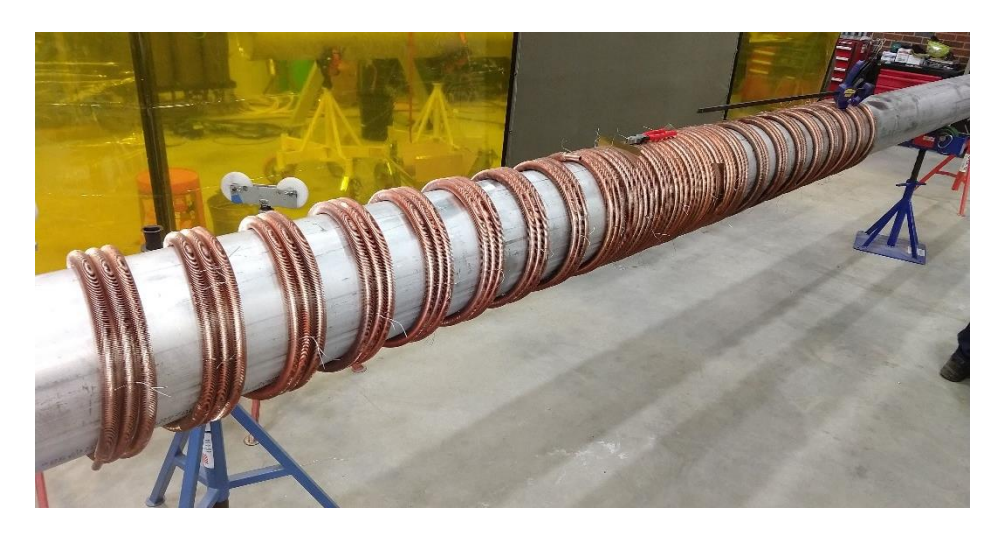


Figure 4.3: Coiled tubes carefully spaced out on the mandrel

The coils were kept together by twisting steel wires around pairs of them at many points around the circumference, as shown in figure 4.4. Once they were tight and tied together, they were unlikely to move out of place because of the friction the fins provide.



Figure 4.4: Tubes tied together with wires and cinched down with sheets and clamps

Another significant difficulty was sliding the shell over the finned tubes once they were in place. There is minimal clearance between the mandrel, tubes, and shell. Again, this is to prevent bypass. The tubes were tightened to the mandrel using thin metal sheets and hose clamps, as shown in figure 4.4, above. This was done along the length of the heat exchanger.

The initial method for sliding the shell on was attaching flanges to the top end of the mandrel (the shell was being slid on from the bottom) and the top end of the shell. All-thread rods were used as bolts. The nuts on the flange on the shell were tightened on two sides simultaneously to pull the shell over the tubes. This process was done a few threads at a time, stopping to make sure the ropes were not getting caught and were staying in place under the shell. The metal sheets were left on the tubes as long as possible to keep them tight to the mandrel. The sheets were

removed, one by one, as the flange approached them. The heat exchanger after the shell was installed is shown in figure 4.5.



Figure 4.5: Heat exchanger with shell installed

As the shell was pushed on, some of the fins stuck out further than the inside diameter of the shell, so they were bent so they would fit inside. This is clearly not ideal. The design was since changed, including larger ropes and a slightly larger shell diameter. This allows more clearance between the fins and the shell, while still blocking bypass. The entire apparatus was mounted equipment that allows it to be rotated. This allows much easier access to the fins and ropes during fabrication.

CHAPTER 5: OPERATIONAL AND MAINTENANCE PROCEDURES

5.1 Modes of Operation

The purifier has several modes of operation for regenerating the adsorbent and heat exchanger. This must be done to avoid surpassing the capacity of these components. A detailed operational scheme is laid out here. This includes P&Is and valve settings for each mode.

- The first mode is Regular Operation. This is the mode that the purifier will be in most of the time, while it is purifying helium.
- The second mode is Helium Blow Down. This step begins the regeneration process. The helium inlet and outlet valves are closed, and a vent is opened to release the potentially dirty helium in the system. The pressure is reduced to approximately 20 psig. This leaves the system at positive pressure, helping with warm-up.
- The third mode is LN2 Evaporation and Warm Up. The fin side of the heat exchanger is isolated. The liquid nitrogen inlet is turned off. Moderate heat is added to the carbon bed, warming it up to approximately 200 K. This boils off the LN2. The rest of the helium in blown down, reducing the system pressure to approximately 1-2 psig.
- The fourth mode is Heating. Heaters are turned on around the carbon bed to heat it up further, to approximately 350 K. Helium is circulated at approximately 0.5 g/s and warmed to approximately ambient temperature by opening it to a vaporizer and a blower circuit.

- The fifth mode is Pump. The helium circulation and heaters are stopped. The shell side of the heat exchanger and the carbon bed are separately pumped down to a vacuum, removing any moisture left in the heat exchanger and regenerating the carbon.
- The sixth mode is Backfill. The shell side of the heat exchanger and the rest of the purifier are separately backfilled with helium to approximately 1-2 psig. This is the first mode of operation when starting up a new purifier, or one that has been unused for some time. Repeat modes 5 and 6 in sequence 3 times.
- The seventh mode is Cool Down and Purge. The purifier circulates helium as if in normal operation, except that it is fed with clean helium. The liquid nitrogen inlet is turned back on. This continues until desired temperatures are reached, then the purifier can be put into regular operation mode.

5.2 Description of Operating and Maintenance Procedures

This section will give a detailed description of purifier operation and maintenance, including P&Is showing flow paths and valve settings. A green-highlighted valve is open (or in operation, for control valves), while a red-highlighted valve is closed. The green streams are nitrogen. The blue streams are helium that has not yet or being purified. The red streams are clean helium, after purification.

5.2.1 Regular Operation

- a) Close the cooldown valves (MV75171 and MV75172)
- b) Verify the blower circuit is closed (MV75154 and MV75156)
- c) Verify the helium vent is closed (MV75153)
- d) Open the helium inlet and outlet valves (MV75111 and MV75119)

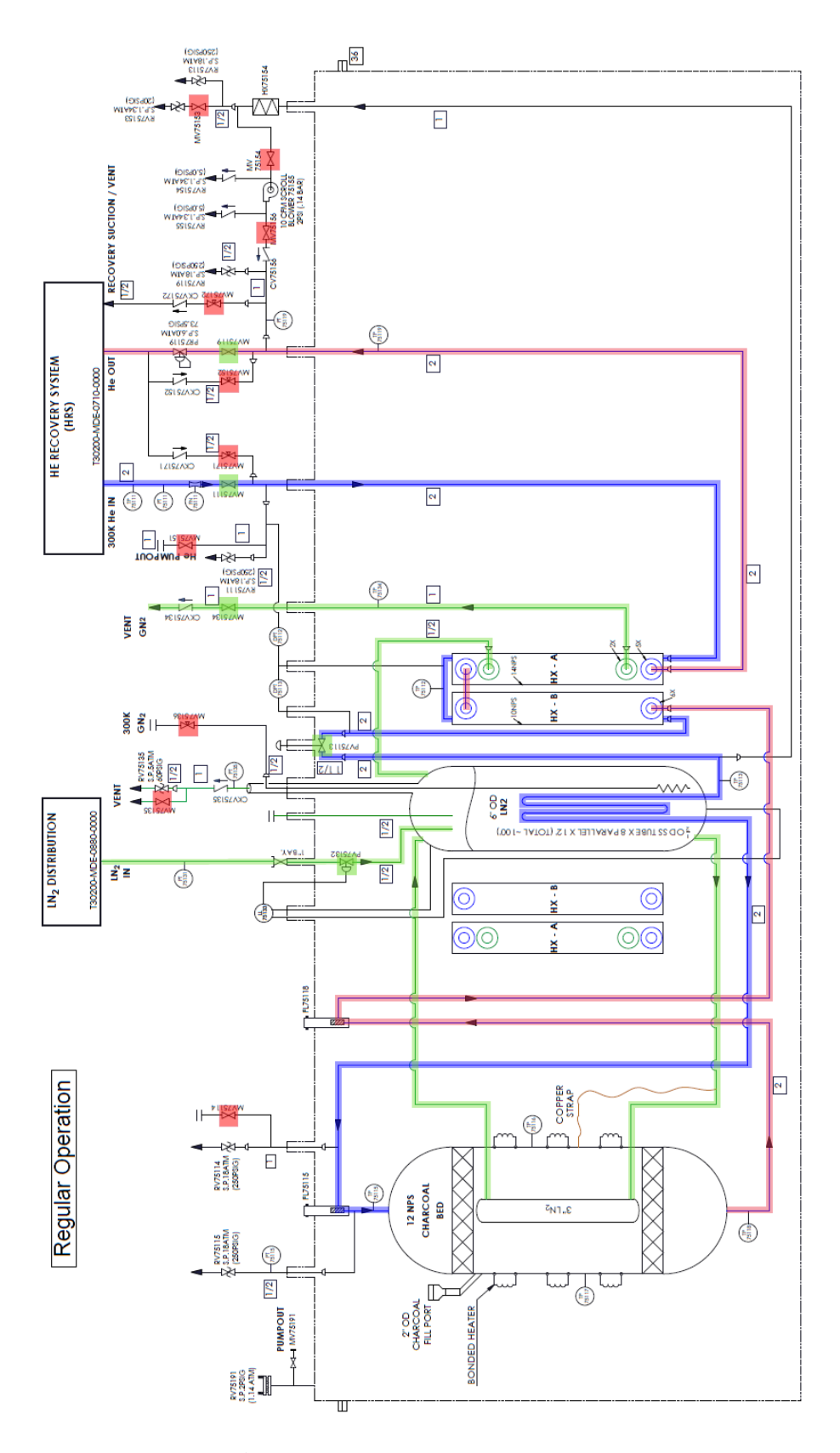


Figure 5.1: Regular Operation P&I

5.2.2 <u>Helium Blow Down</u>

- a) Make sure the compressor discharge is aligned to the other purifier.
- b) Shut the helium inlet valve (MV75111)
- c) Shut the helium outlet valve (MV 75119)
- d) Open the blow down valve (MV75153)
- e) Verify LN2 is on (PV75132)
- f) Verify the inlet to the blower is closed (MV75154)

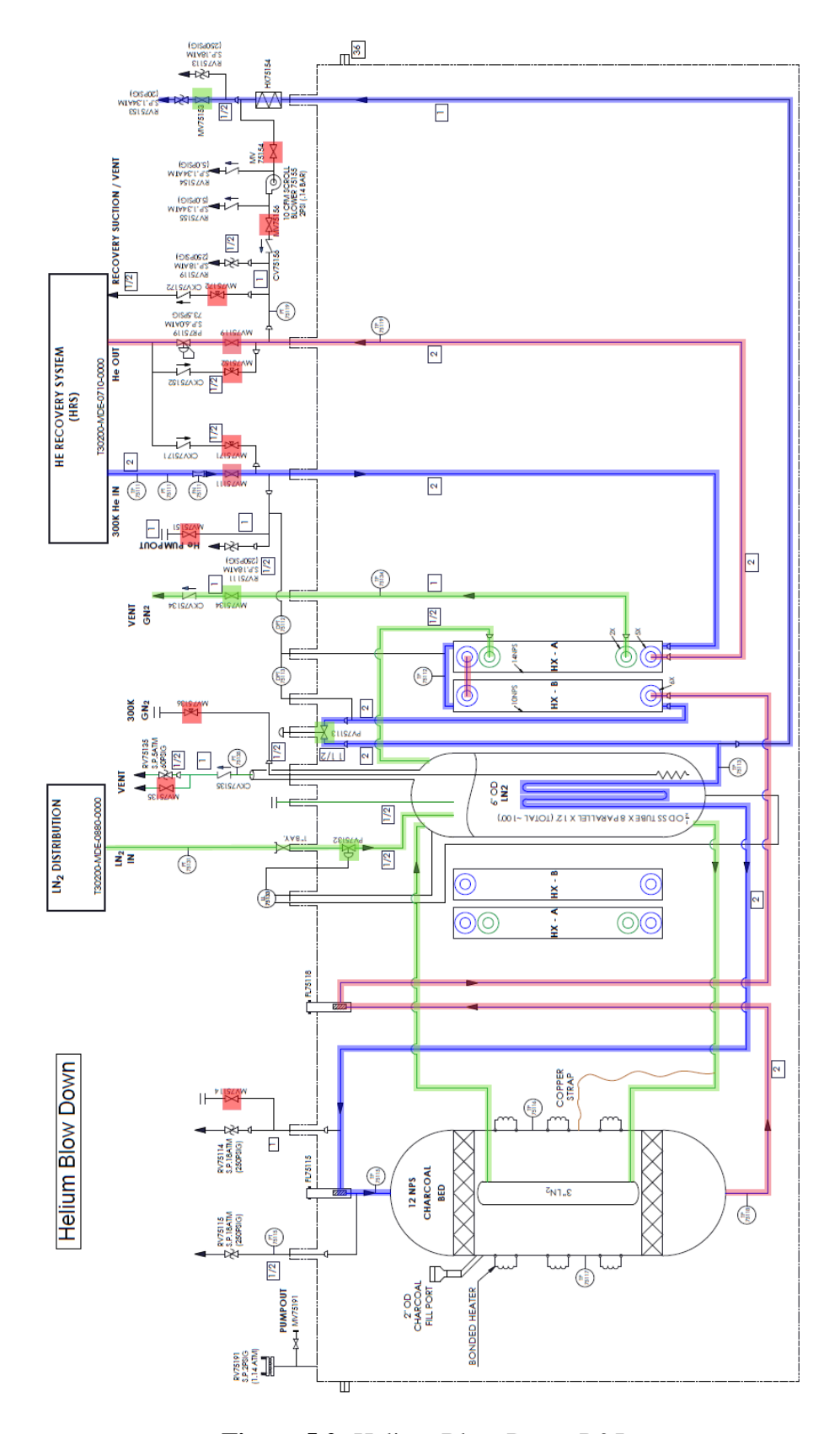


Figure 5.2: Helium Blow Down P&I

5.2.3 <u>LN2 Evaporation and Warm Up</u>

- a) Isolate the fin side of the heat exchanger, close PV75113
- b) Close the LN2 inlet control valve (PV75132)
- c) Open the nitrogen boiler vent (MV75135)
- d) Close the heat exchanger nitrogen vent (MV75134)
- e) Slowly open the GN2 as needed to evaporate LN2 (MV75136)
- f) Begin blower cycle
 - a. Open MV75154 and MV75156
 - b. Turn on blower
 - c. Turn on heater so the carbon bed reaches 200 K

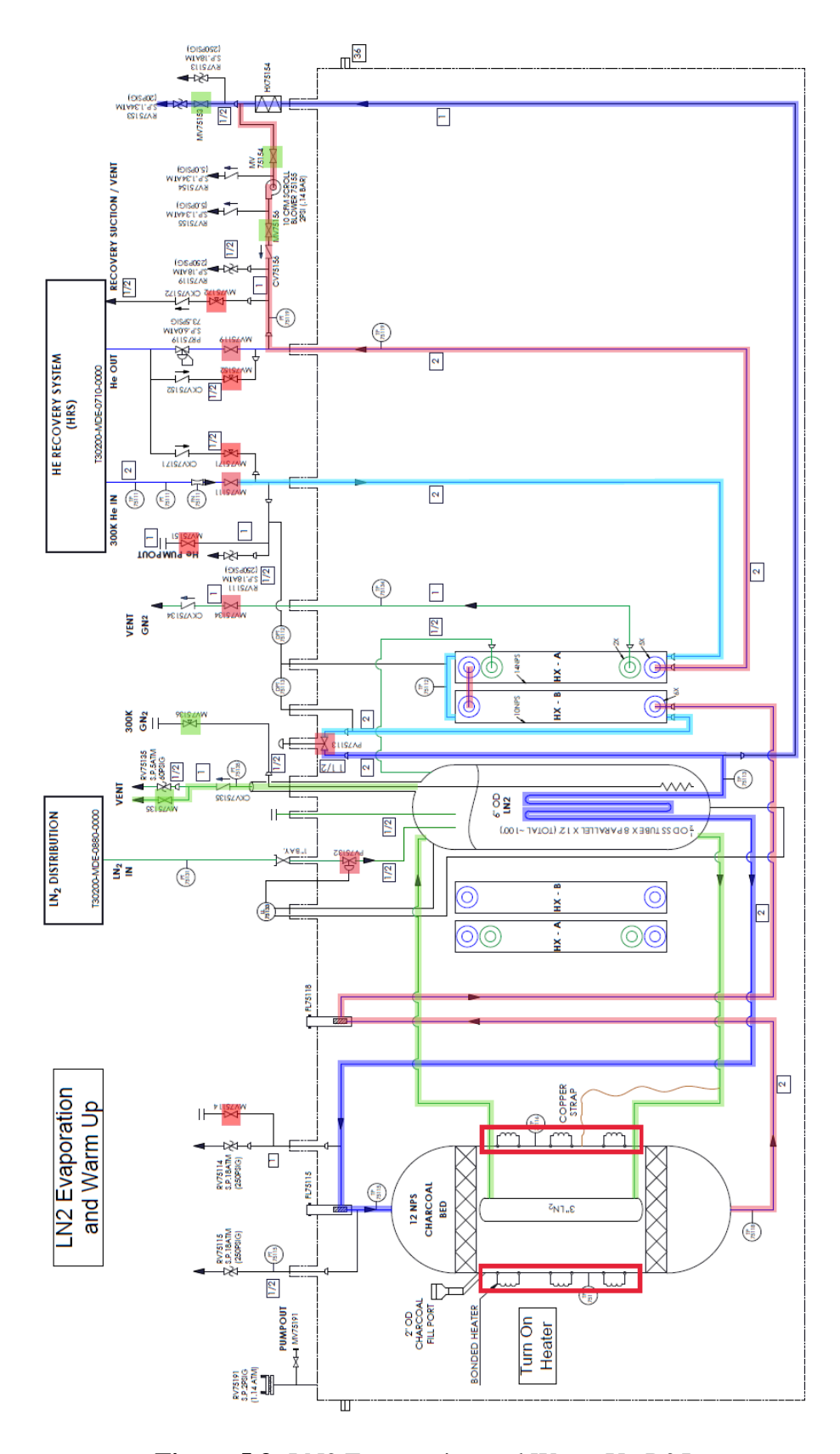


Figure 5.3: LN2 Evaporation and Warm Up P&I

5.2.4 <u>Heating</u>

- a) Verify that the GN2 inlet is closed (MV75136)
- b) Turn heater up so the carbon bed reaches $350\;\mathrm{K}$

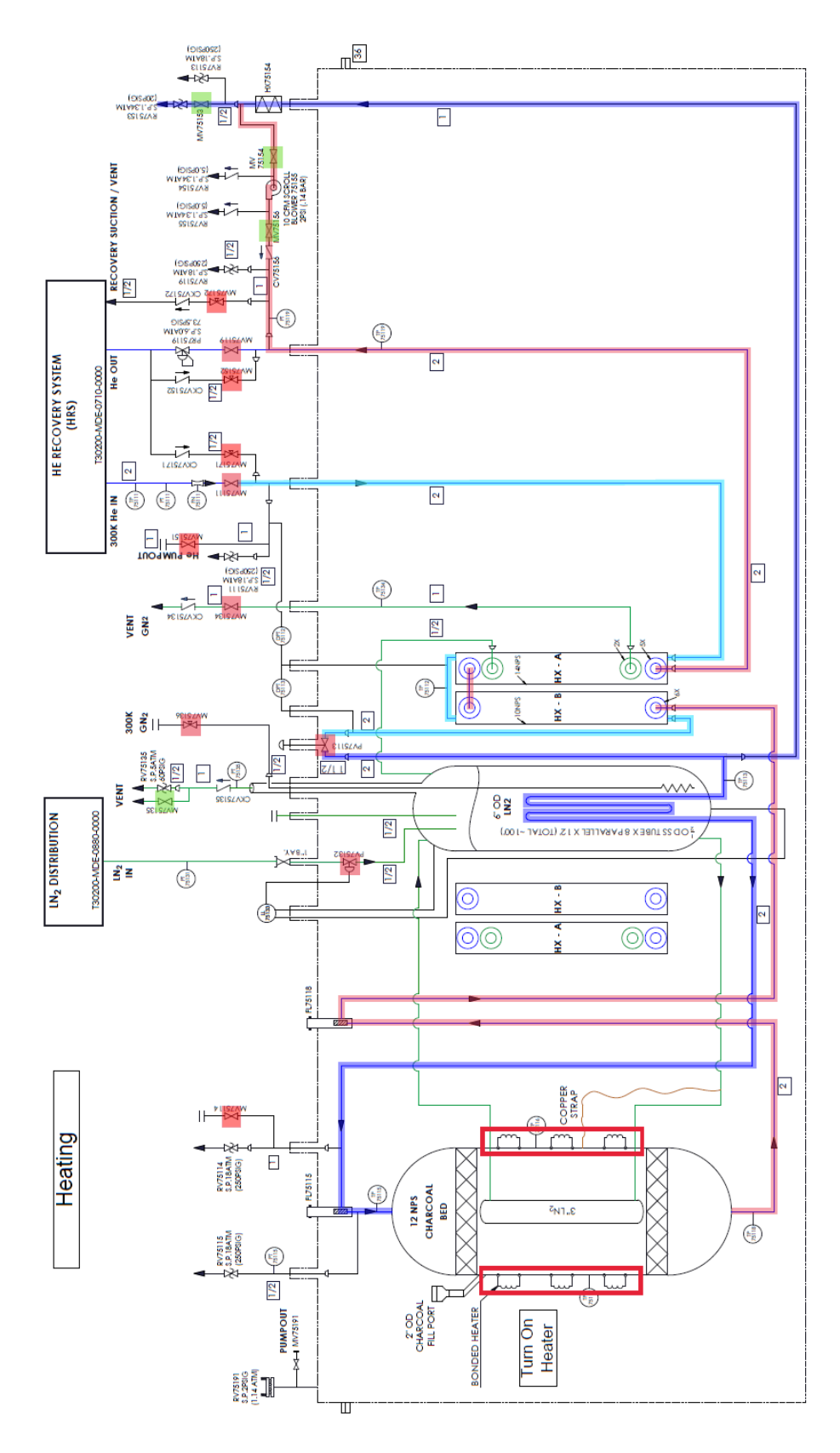


Figure 5.4: Heating P&I

5.2.5 <u>Pump</u>

- a) Turn off the heat, and blower
- b) Close MV75153, MV75154, and MV75156
- c) Close backfill valves if open (MV75151 and MV75114)
- d) Verify that all valves that need to be closed are, so there is no unwanted gas in the system
 - a. Especially MV75113 (it separates the fin side of the heat exchanger)
- e) Verify that the cold trap is clean and in place
- f) Verify that the vacuum pump(s) is attached to both ports properly
- g) Slowly open the vacuum valves (MV75151 and MV75114)
 - a. Close when pressure stops reducing

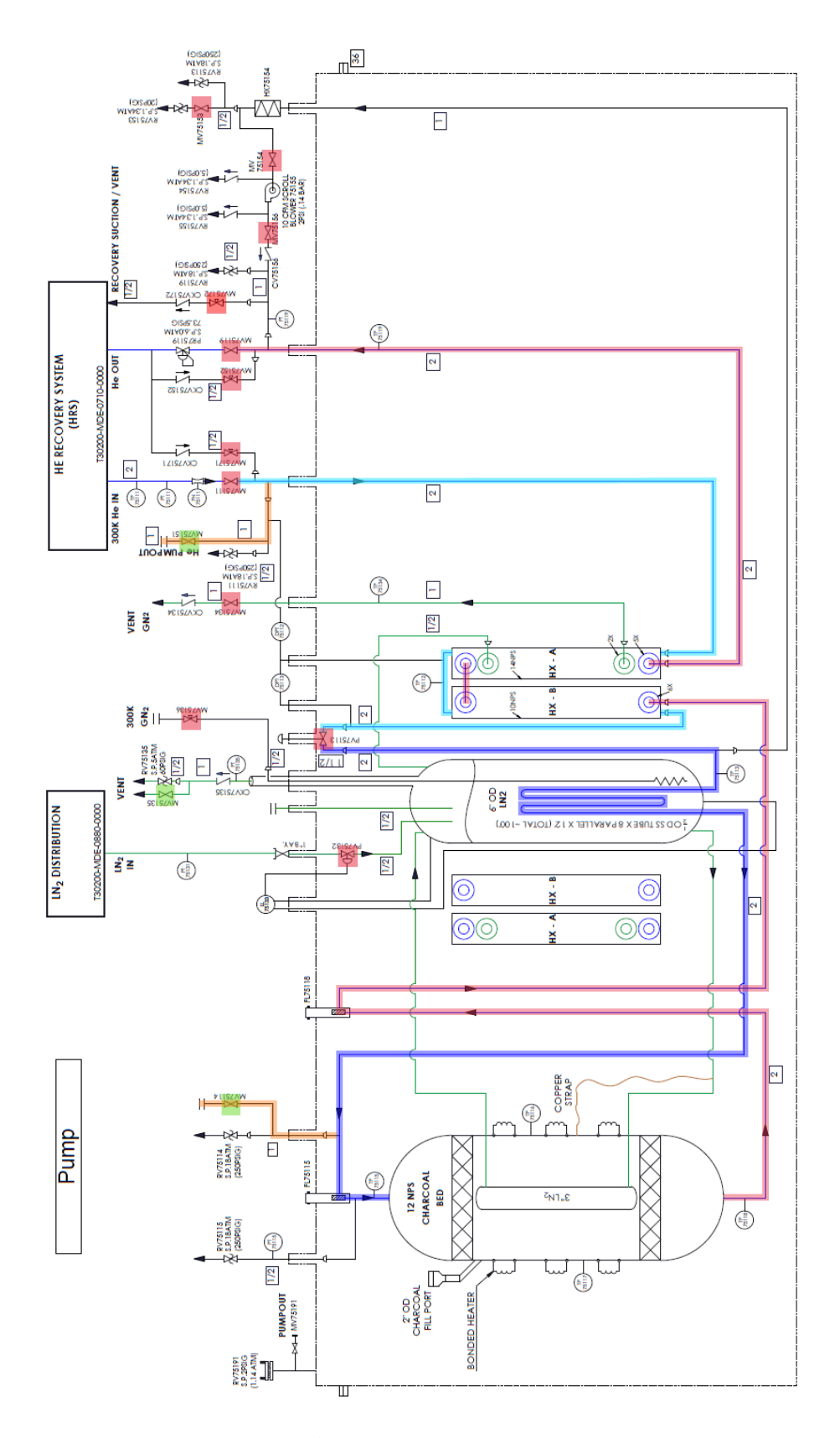


Figure 5.5: Pump P&I

5.2.6 <u>Backfill</u>

- a) Close the vacuum valves (MV75151 and MV75114)
- b) Slowly open the purifier backfill valves (MV75152 and MV75171)
 - a. Close when pressure gets to the designated pressure (1-2 psig)
- c) Repeat steps Pump (5.2.5) and Backfill (5.2.6), in sequence, three times or until the baseline pressure (pressure after pumping) stops reducing between repetitions

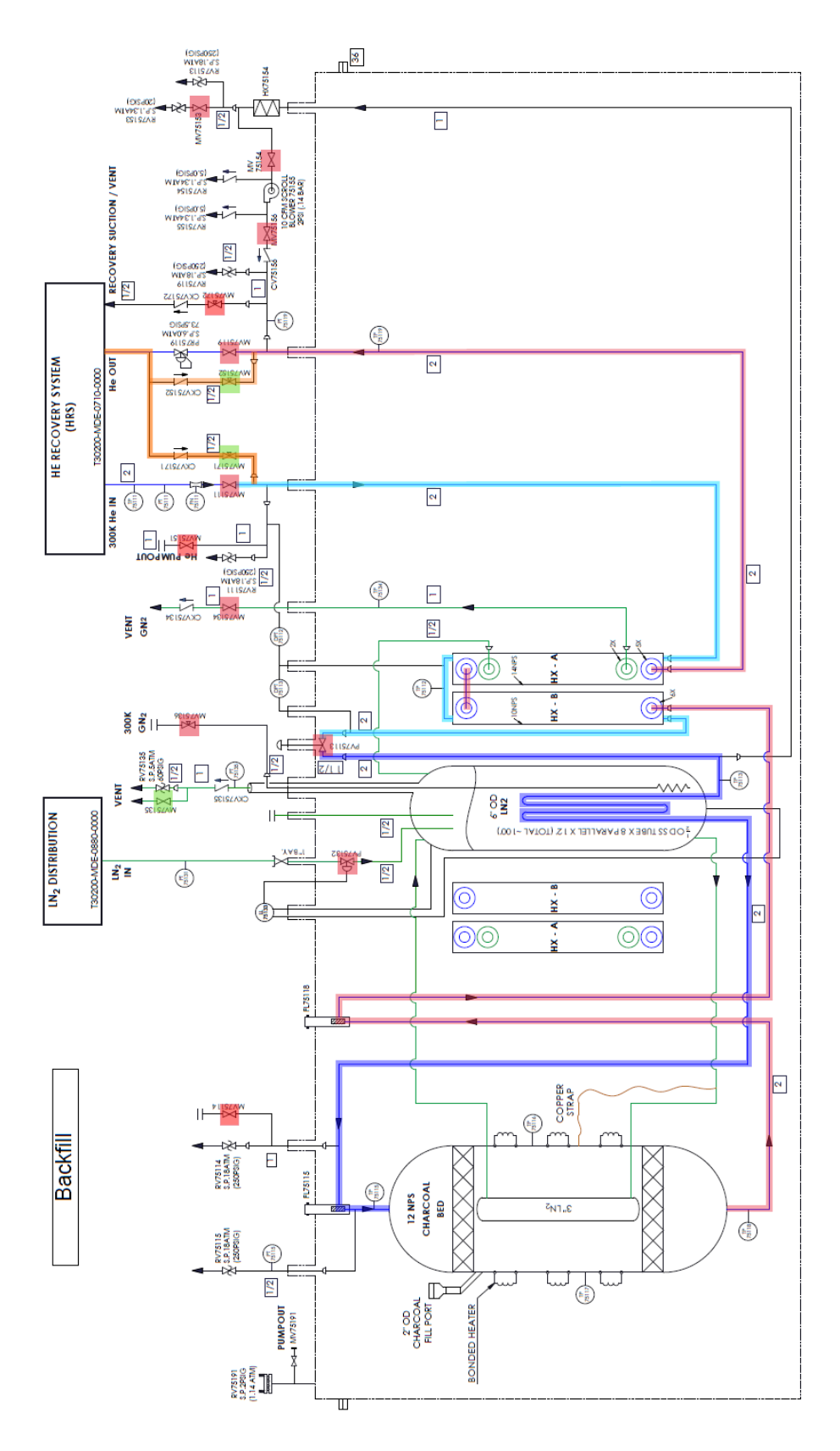


Figure 5.6: Backfill P&I

5.2.7 <u>Cooldown</u>

- a) Close heat exchanger shell side backfill valve if open (MV75152)
- b) Open the heat exchanger nitrogen vent (MV75134)
- c) Close the nitrogen boiler vent (MV75135)
- d) Turn on the LN2 inlet control valve (PV75132)
- e) Open the heat exchanger shell side to the rest of the purifier (MV75113)
- f) Open the cooldown return valve (MV75172)
- g) Open the cooldown supply valve (MV75171)
- h) When all the temperatures are where they need to be, transition into purification mode

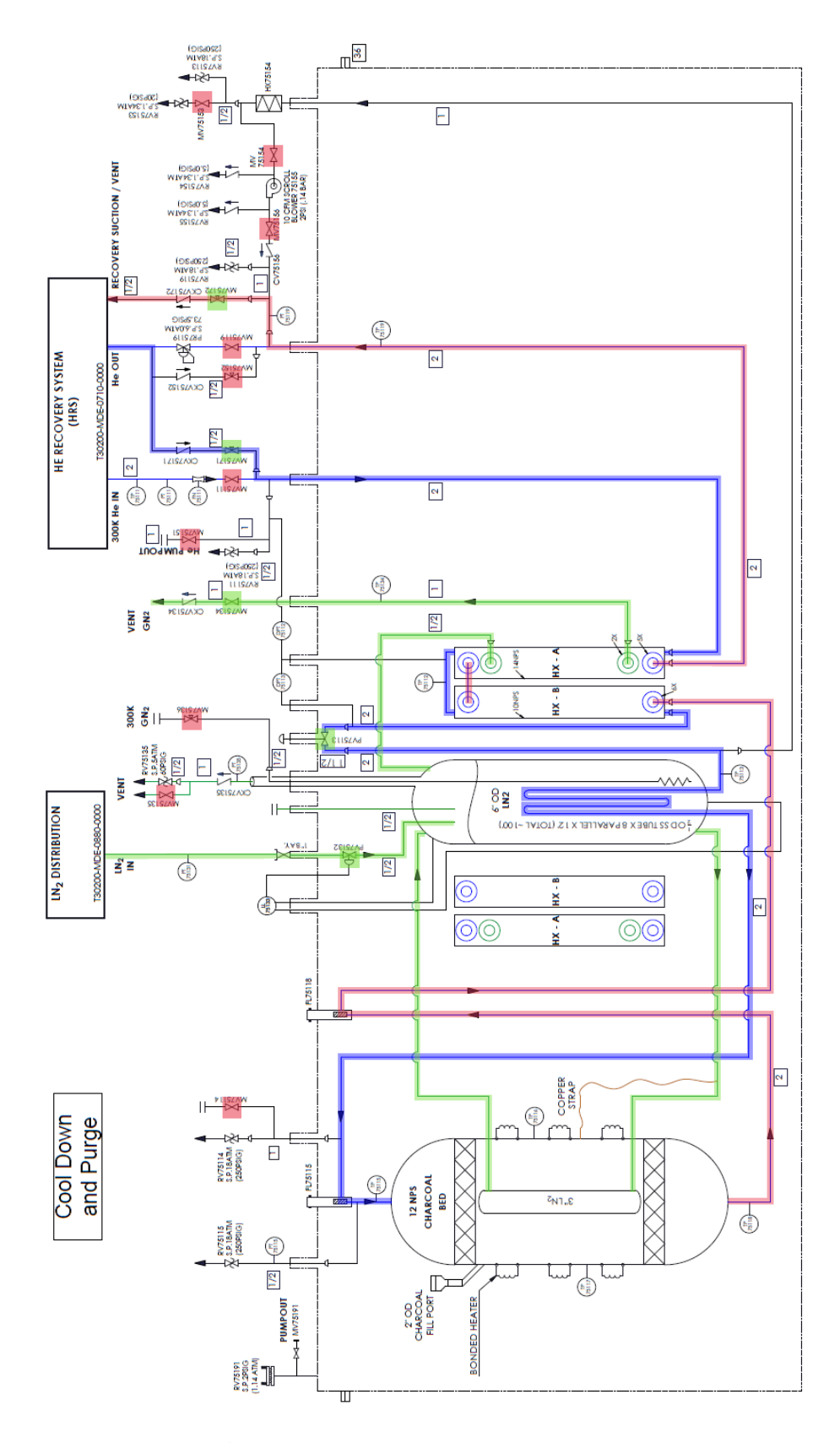


Figure 5.7: Cool Down and Purge P&I

5.3 Valve Position Matrix

The matrix in figure 5.8 shows the physical positions of the valves as they will be on the valve rack. It also shows the progression of the valves during operation and regeneration.

Regular Operation										
Operation	11	19	34		13	32				
Warm Up	53	54	56		Heater	Blower				
Pump	Vacuum	51	14							
Backfill & Purge	52	71	72							
N2 Warm Up	35	36								

Back	ground					
Green	Open					
White	Closed					
1	ext					
Yellow	Opening					
Red	Closing					

Helium Blow Down									
Operation	11	19	34		13	32			
Warm Up	53	54	56		Heater	Blower			
Pump	Vacuum	51	14]					
Backfill & Purge	52	71	72]					
N2 Warm Up	35	36							

LN2 Evaporation and Warm Up									
Operation	11	19	34		13	32			
Warm Up	53	54	56		Heater	Blower			
Pump	Vacuum	51	14						
Backfill & Purge	52	71	72						
N2 Warm Up	35	36							

	Heating										
Operation	11	19	34		13	32					
Warm Up	53	54	56		Heater	Blower					
Pump	Vacuum	51	14								
Backfill & Purge	52	71	72								
N2 Warm Up	35	36									

	Pump										
Operation	11	19	34		13	32					
Warm Up	53	54	56		Heater	Blower					
Pump	Vacuum	51	14								
Backfill & Purge	52	71	72								
N2 Warm Up	35	36									

Backfi	Backfill (Repeat Pump and Backfill at least 3 times)										
Operation 11 19 34 13											
Warm Up	53	54	56		Heater	Blower					
Pump	Vacuum	51	14								
Backfill & Purge	52	71	72								
N2 Warm Up 35 36											

Cool Down and Purge										
Operation	11	19	34		13	32				
Warm Up	53	54	56		Heater	Blower				
Pump	Vacuum	51	14							
Backfill & Purge	52	71	72							
N2 Warm Up	35	36								

Figure 5.8: Valve position matrix

CHAPTER 6: SUMMARY AND CONCLUSION

The design of a helium purification system utilizing a freeze-out heat exchanger for application in systems requiring helium refrigeration is reported. The purification system is designed to remove low level air impurities. This is done using freeze-out purification to remove moisture and adsorption purification to remove air. Key features of the process design, mechanical design, fabrication, and operation procedures are discussed is this paper. The most critical tasks of the design were the pressure design (especially of shells) and physical design for facilitating simple fabrication. The fabrication of a prototype of the heat exchanger greatly assisted this. It showed the limitations of the design and solutions were found to overcome those limitations, namely larger clearance between the finned tubes and the shell, larger ropes, and a rotatable fixture for holding the apparatus. The process design included heat exchanger design, and component selection and sizing. The mechanical design included design and stress analysis of vessels, heads, and piping. Detailed analysis of the purification system demonstrates an effective and efficient design for supporting the 6-16 bar operation, with operating period of at least 22 days at a design contamination level of 30 ppm in 30 g/s of helium and an LN consumption of approx. 0.05 m³/hr. at full capacity. This design and analysis has shown that this purifier can be a good tool to serve as the primary helium purification system for MSU-FRIB cryogenic refrigerator and superconducting magnet test facility.

APPENDICES

APPENDIX A: STRESS ANALYSIS

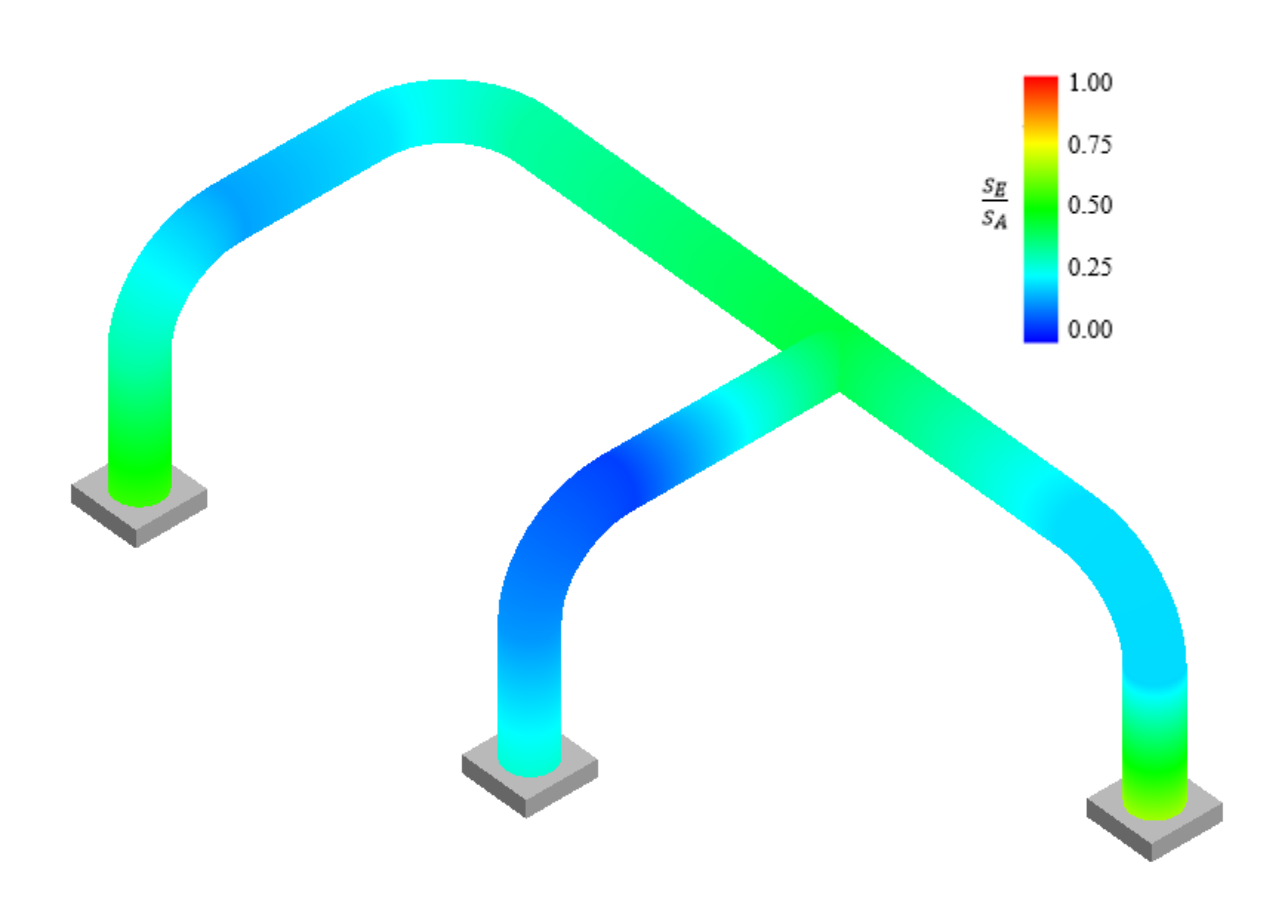


Figure A.1: CAEPIPE model of nitrogen piping from nitrogen boiler to heat exchanger

Table A.1: CAEPIPE B31.3 code compliance for nitrogen piping from nitrogen boiler to heat exchanger

		Sust	ained			Expar	nsion	
#	Node	SL (psi)	SH (psi)	SL SH	Node	SE (psi)	SA (psi)	SE SA
1	110	438	20000	0.02	190	20686	30000	0.69
2	100B	438	20000	0.02	120	17079	30000	0.57
3	120	430	20000	0.02	50	13289	30000	0.44
4	10	424	20000	0.02	100B	10313	30000	0.34
5	180	420	20000	0.02	110	10313	30000	0.34
6	170B	420	20000	0.02	70A	10126	30000	0.34
7	100A	417	20000	0.02	60	10125	30000	0.34
8	90	417	20000	0.02	10	9093	30000	0.30
9	30A	416	20000	0.02	70B	6763	30000	0.23
10	20	416	20000	0.02	80	6762	30000	0.23
11	50	413	20000	0.02	170A	6575	30000	0.22
12	190	406	20000	0.02	130	6574	30000	0.22
13	130	401	20000	0.02	170B	6425	30000	0.21
14	170A	401	20000	0.02	180	6424	30000	0.21
15	40	396	20000	0.02	100A	4782	30000	0.16
16	30B	396	20000	0.02	90	4782	30000	0.16
17	70A	396	20000	0.02	30A	4528	30000	0.15
18	60	396	20000	0.02	20	4528	30000	0.15
19	70B	389	20000	0.02	30B	1850	30000	0.06
20	80	389	20000	0.02	40	1850	30000	0.06

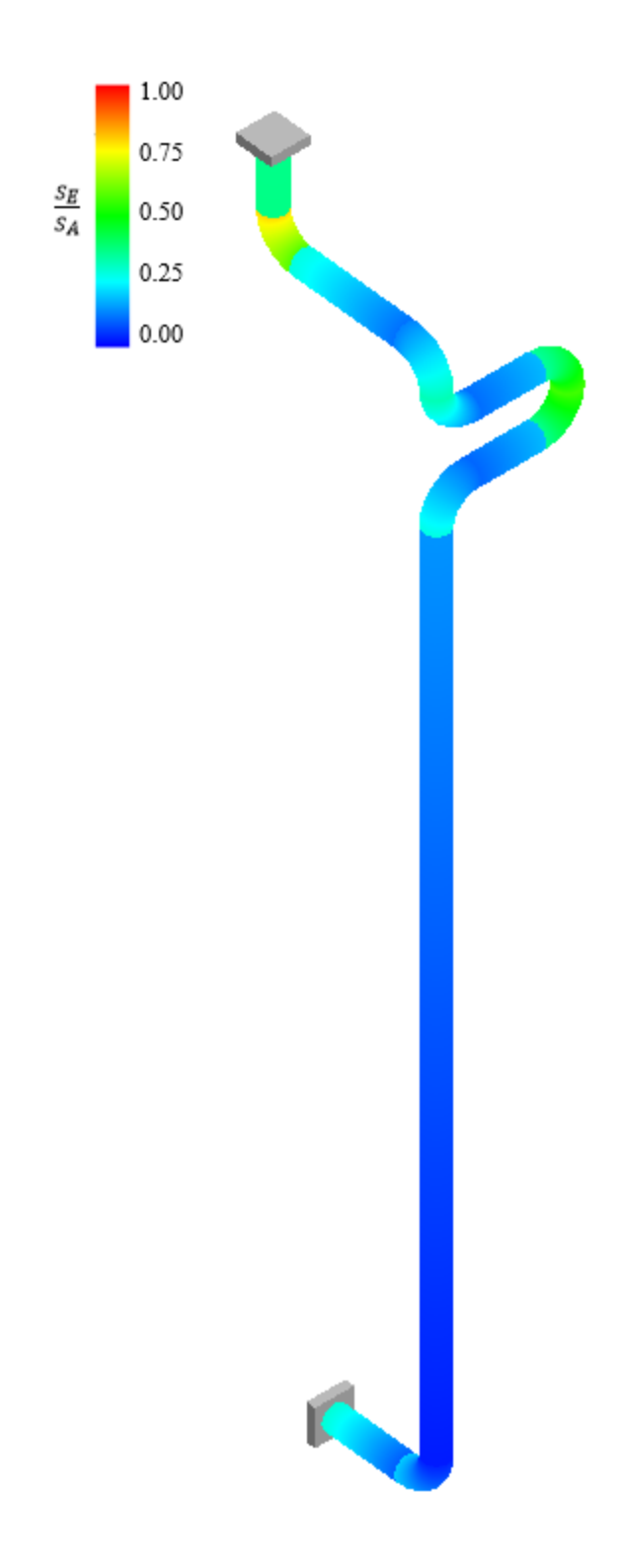


Figure A.2: Stress distribution for helium piping from supply to the heat exchanger

Table A.2: CAEPIPE B31.3 code compliance for helium piping from supply to the heat exchanger

		Susta	ained			Expar	nsion	
#	Node	SL (psi)	SH (psi)	SL SH	Node	SE (psi)	SA (psi)	SE_SA
1	10	1472	20000	0.07	100B	23630	30000	0.79
2	100B	996	20000	0.05	100A	17488	30000	0.58
3	30A	982	20000	0.05	54B	16916	30000	0.56
4	30B	949	20000	0.05	56A	16916	30000	0.56
5	51A	946	20000	0.05	110	11077	30000	0.37
6	100A	929	20000	0.05	120	10937	30000	0.36
7	110	928	20000	0.05	54A	10720	30000	0.36
8	120	921	20000	0.05	56B	10340	30000	0.34
9	20	916	20000	0.05	70A	9688	30000	0.32
10	54B	902	20000	0.05	59B	9576	30000	0.32
11	56A	902	20000	0.05	10	9157	30000	0.31
12	70A	897	20000	0.04	90	8404	30000	0.28
13	50	892	20000	0.04	51A	8339	30000	0.28
14	59B	887	20000	0.04	30A	6077	30000	0.20
15	51B	887	20000	0.04	53	5533	30000	0.18
16	90	885	20000	0.04	57	5482	30000	0.18
17	40	883	20000	0.04	50	4347	30000	0.14
18	70B	874	20000	0.04	70B	3821	30000	0.13
19	56B	865	20000	0.04	59A	3436	30000	0.11
20	52	859	20000	0.04	80	3327	30000	0.11
21	54A	858	20000	0.04	58	3243	30000	0.11
22	80	852	20000	0.04	51B	3099	30000	0.10
23	59A	849	20000	0.04	52	2998	30000	0.10
24	57	847	20000	0.04	20	2773	30000	0.09
25	53	842	20000	0.04	30B	1028	30000	0.03
26	58	837	20000	0.04	40	759	30000	0.03

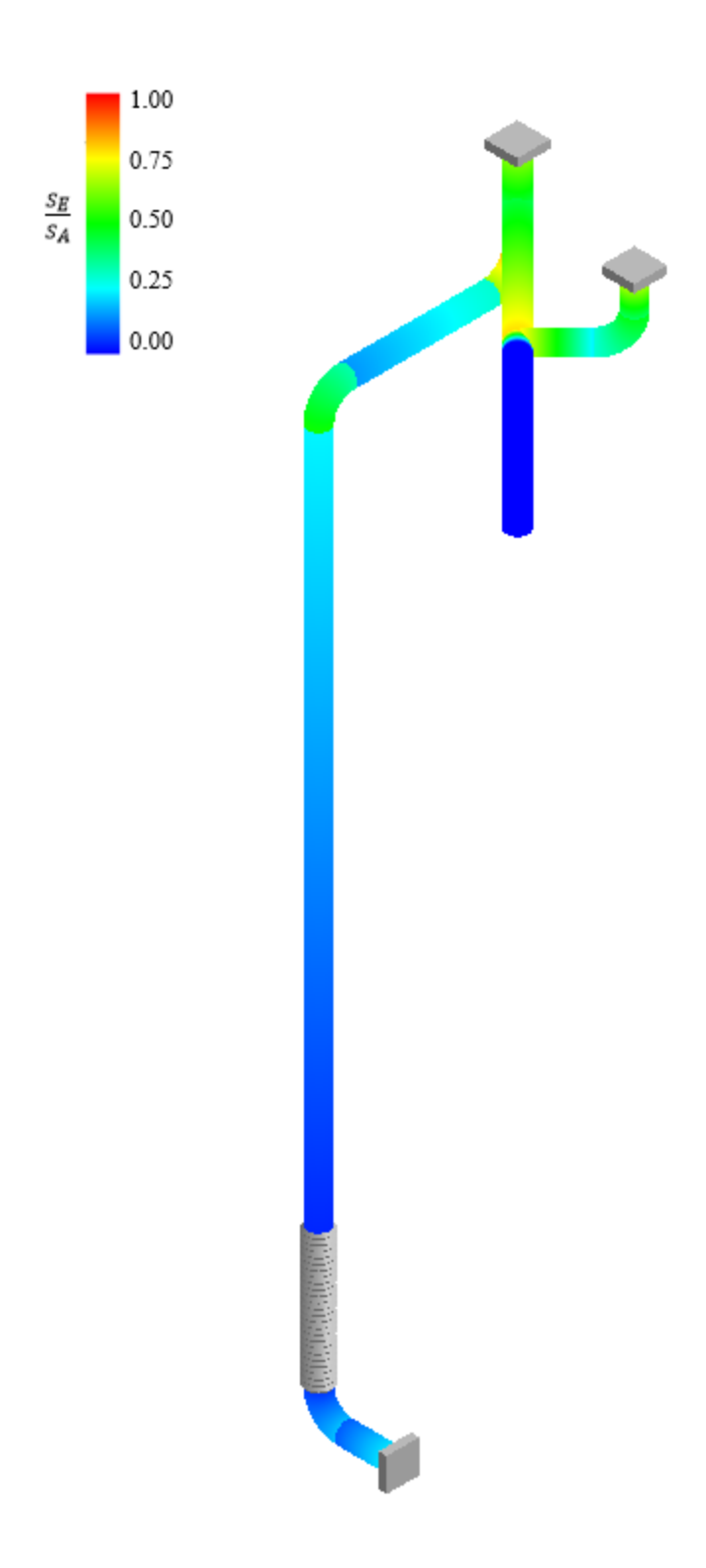


Figure A.3: Stress distribution for helium piping from the heat exchanger to the nitrogen boiler

Table A.3: CAEPIPE B31.3 code compliance for helium piping from the heat exchanger to the nitrogen boiler

		Susta	ained			Expar	nsion	
#		SL	SH	SL		SE	SA	SE SA
	Node	(psi)	(psi)	SH	Node	(psi)	(psi)	SA
1	10	1346	20000	0.07	90B	25190	30000	0.84
2	30A	1102	20000	0.06	130	23414	30000	0.78
3	20	988	20000	0.05	170	22454	30000	0.75
4	150B	957	20000	0.05	120	20068	30000	0.67
5	120	952	20000	0.05	90A	19630	30000	0.65
6	110	947	20000	0.05	60A	15437	30000	0.51
7	160	908	20000	0.05	150B	14364	30000	0.48
8	170	905	20000	0.05	110	12581	30000	0.42
9	130	879	20000	0.04	160	12193	30000	0.41
10	150A	864	20000	0.04	100	11635	30000	0.39
11	190A	860	20000	0.04	60B	9874	30000	0.33
12	90B	855	20000	0.04	80	8900	30000	0.30
13	60B	854	20000	0.04	150A	8844	30000	0.29
14	140	847	20000	0.04	10	7472	30000	0.25
15	180	843	20000	0.04	55	7231	30000	0.24
16	100	842	20000	0.04	140	6856	30000	0.23
17	70	840	20000	0.04	30A	5653	30000	0.19
18	60A	829	20000	0.04	70	4503	30000	0.15
19	55	823	20000	0.04	20	2674	30000	0.09
20	90A	821	20000	0.04	30B	1642	30000	0.05
21	190B	821	20000	0.04	50	1075	30000	0.04
22	200	821	20000	0.04	190A	0	30000	1.00
23	80	820	20000	0.04	180	0	30000	0.00
24	210	817	20000	0.04	190B	0	30000	0.00
25	30B	799	20000	0.04	210	0	30000	0.00
26	50	795	20000	0.04	200	0	30000	0.00

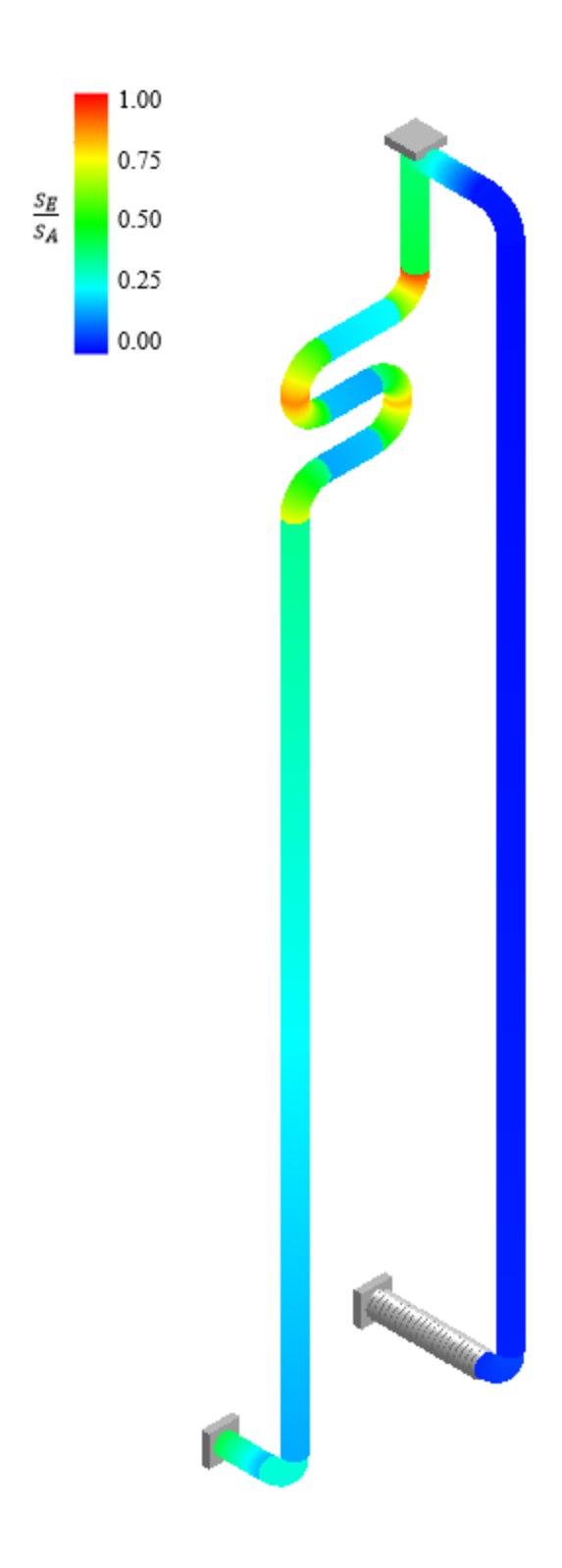


Figure A.4: Stress distribution for helium piping from the nitrogen boiler to the carbon bed

Table A.4: CAEPIPE B31.3 code compliance for helium piping from the nitrogen boiler to the carbon bed

		Susta	ained			Expar	nsion	
#		SL	SH	SL SH		SE	SA	SE SA
	Node	(psi)	(psi)		Node	(psi)	(psi)	
1	80	1606	20000	0.08	110A	28346	30000	0.94
2	90	1605	20000	0.08	140B	26039	30000	0.87
3	190	1379	20000	0.07	151A	26039	30000	0.87
4	170B	1053	20000	0.05	154B	24316	30000	0.81
5	60B	1023	20000	0.05	156A	24316	30000	0.81
6	60A	1023	20000	0.05	159B	22295	30000	0.74
7	110A	998	20000	0.05	110B	16757	30000	0.56
8	180	959	20000	0.05	140A	14457	30000	0.48
9	50	957	20000	0.05	190	13897	30000	0.46
10	70	941	20000	0.05	100	13324	30000	0.44
11	100	930	20000	0.05	156B	12732	30000	0.42
12	151A	926	20000	0.05	151B	12585	30000	0.42
13	140B	926	20000	0.05	80	11730	30000	0.39
14	110B	909	20000	0.05	90	11543	30000	0.38
15	151B	902	20000	0.05	154A	10863	30000	0.36
16	170A	898	20000	0.04	159A	10714	30000	0.36
17	156A	897	20000	0.04	1591	10591	30000	0.35
18	154B	897	20000	0.04	170A	8675	30000	0.29
19	154A	888	20000	0.04	170B	8625	30000	0.29
20	159B	884	20000	0.04	120	7615	30000	0.25
21	140A	877	20000	0.04	130	6577	30000	0.22
22	156B	874	20000	0.04	157	5793	30000	0.19
23	120	873	20000	0.04	152	5729	30000	0.19
24	152	868	20000	0.04	180	5306	30000	0.18
25	153	860	20000	0.04	160	4972	30000	0.17
26	1591	855	20000	0.04	153	4951	30000	0.17
27	130	853	20000	0.04	158	4882	30000	0.16
28	157	852	20000	0.04	30B	1962	30000	0.07
29	160	851	20000	0.04	30A	1259	30000	0.04
30	159A	839	20000	0.04	40	918	30000	0.03
31	30B	836	20000	0.04	60B	717	30000	0.02
32	158	830	20000	0.04	60A	407	30000	0.01
33	40	830	20000	0.04	70	368	30000	0.01
34	30A	821	20000	0.04	50	246	30000	0.01
	-					-		

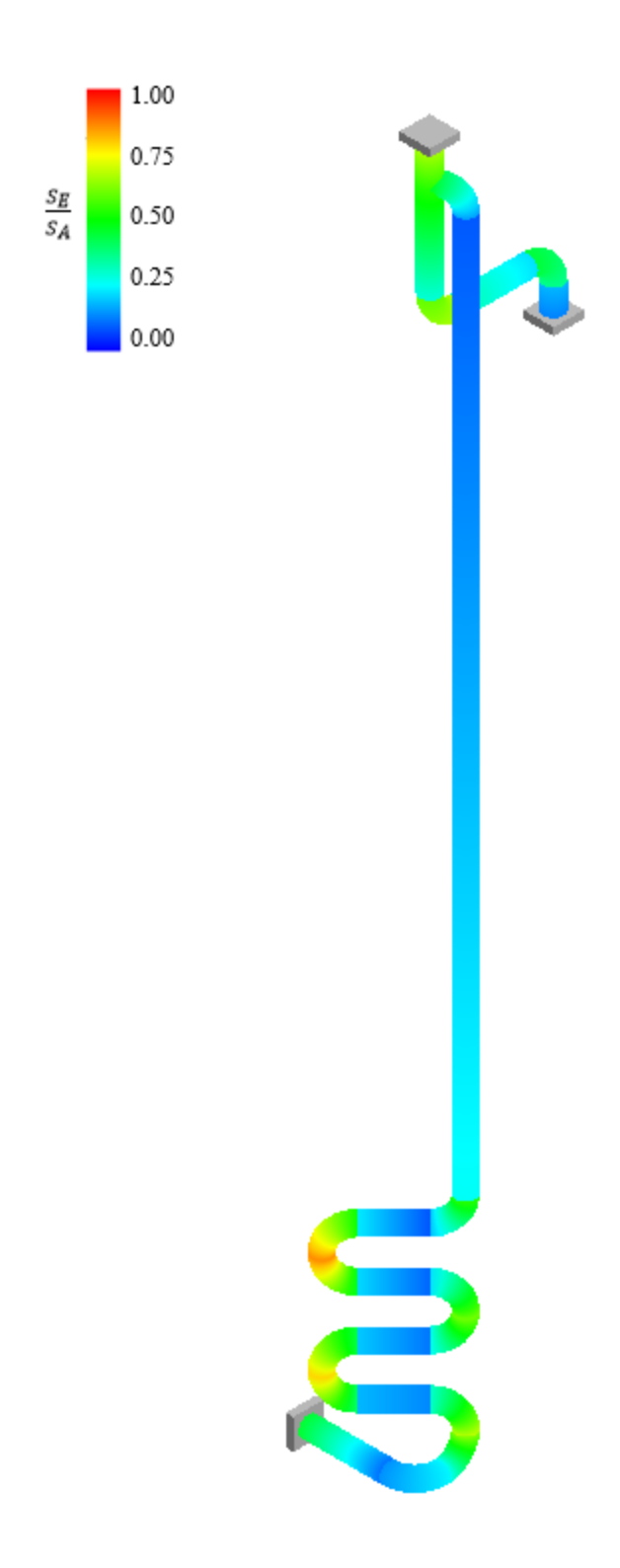


Figure A.5: Stress distribution for helium piping from the carbon bed to the heat exchanger

Table A.5: CAEPIPE B31.3 code compliance for helium piping from the carbon bed to the heat exchanger

		Susta	ained			Expar	nsion	
#		SL	SH	SL		SE	SA	SE
	Node	(psi)	(psi)	SH	Node	(psi)	(psi)	SA
1	110B	1195	20000	0.06	74B	25902	30000	0.86
2	10	1094	20000	0.05	76A	25902	30000	0.86
3	120	1046	20000	0.05	64B	23675	30000	0.79
4	130	998	20000	0.05	66A	23675	30000	0.79
5	61A	997	20000	0.05	130	20942	30000	0.70
6	79B	984	20000	0.05	61A	20566	30000	0.69
7	50B	981	20000	0.05	150B	20494	30000	0.68
8	74B	928	20000	0.05	50B	19029	30000	0.63
9	76A	928	20000	0.05	69B	18339	30000	0.61
10	61B	923	20000	0.05	71A	18339	30000	0.61
11	80	922	20000	0.05	150A	17965	30000	0.60
12	64B	909	20000	0.05	79B	16113	30000	0.54
13	66A	909	20000	0.05	120	15978	30000	0.53
14	79A	896	20000	0.04	76B	15321	30000	0.51
15	110A	892	20000	0.04	110B	14320	30000	0.48
16	74A	884	20000	0.04	74A	14208	30000	0.47
17	62	880	20000	0.04	10	14162	30000	0.47
18	100	879	20000	0.04	180A	13306	30000	0.44
19	76B	874	20000	0.04	66B	13095	30000	0.44
20	66B	870	20000	0.04	6 4 A	11982	30000	0.40
21	78	865	20000	0.04	180B	10757	30000	0.36
22	64A	859	20000	0.04	160	9855	30000	0.33
23	73	857	20000	0.04	61B	8872	30000	0.30
24	200	852	20000	0.04	140	8612	30000	0.29
25	77	852	20000	0.04	69A	7759	30000	0.26
26	180A	849	20000	0.04	80	7741	30000	0.26
27	67	849	20000	0.04	50A	7657	30000	0.26
28	50A	845	20000	0.04	30B	7299	30000	0.24
29	71B	843	20000	0.04	77	6926	30000	0.23
30	63	842	20000	0.04	71B	6646	30000	0.22
31	30B	841	20000	0.04	170	6614	30000	0.22
32	150A	840	20000	0.04	73	6423	30000	0.21
33	170	840	20000	0.04	67	5921	30000	0.20
34	180B	838	20000	0.04	79A	5534	30000	0.18
35	140	835	20000	0.04	63	5418	30000	0.18
36	71A	833	20000	0.04	190	5373	30000	0.18
37	69B	833	20000	0.04	110A	4595	30000	0.15
38	72	833	20000	0.04	30A	4256	30000	0.14
39	30A	832	20000	0.04	62	4013	30000	0.13
40	190	829	20000	0.04	200	3585	30000	0.12
41	20	828	20000	0.04	68	3510	30000	0.12
42	150B	828	20000	0.04	20	3295	30000	0.12
43	160	825	20000	0.04	72	3008	30000	0.10
44	69A	820	20000	0.04	100	2614	30000	0.09
45	68	819	20000	0.04	78	2507	30000	0.03
45	00	013	20000	0.04	70	2307	30000	0.00

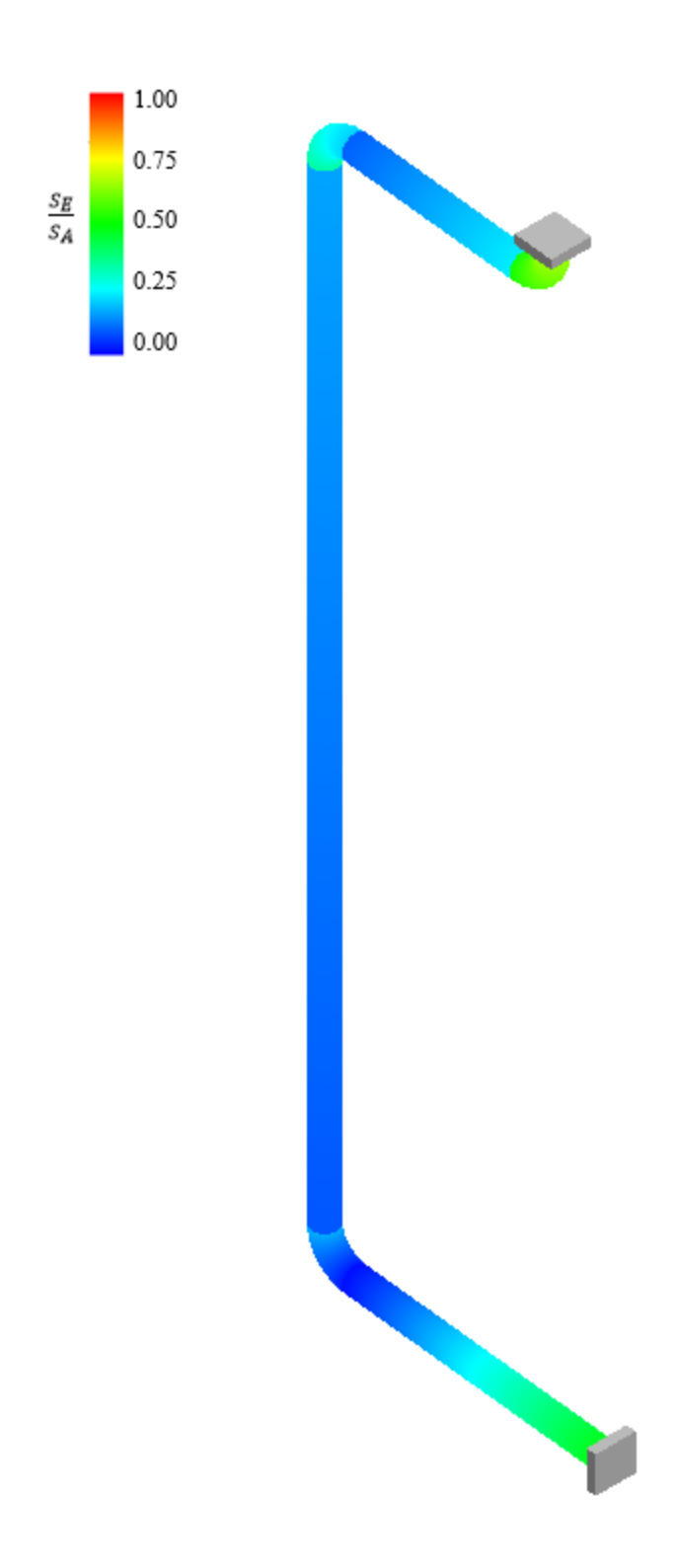


Figure A.6: Stress distribution for helium piping from the heat exchanger to the recovery system

Table A.6: CAEPIPE B31.3 code compliance for helium piping from the heat exchanger to the recovery system

		Susta	ained			Expar	nsion	
#	Node	SL (psi)	SH (psi)	SL SH	Node	SE (psi)	SA (psi)	SE SA
1	10	1840	20000	0.09	90B	19592	30000	0.65
2	90B	1402	20000	0.07	90A	15510	30000	0.52
3	90A	1245	20000	0.06	10	14625	30000	0.49
4	60A	1233	20000	0.06	60A	10277	30000	0.34
5	30B	1217	20000	0.06	100	9025	30000	0.30
6	100	1177	20000	0.06	110	8999	30000	0.30
7	110	1172	20000	0.06	80	7012	30000	0.23
8	60B	1147	20000	0.06	60B	6195	30000	0.21
9	80	1076	20000	0.05	30B	5187	30000	0.17
10	50	1072	20000	0.05	50	4818	30000	0.16
11	30A	1071	20000	0.05	70	2805	30000	0.09
12	40	1050	20000	0.05	40	2519	30000	0.08
13	70	1017	20000	0.05	30A	770	30000	0.03
14	20	969	20000	0.05	20	355	30000	0.01

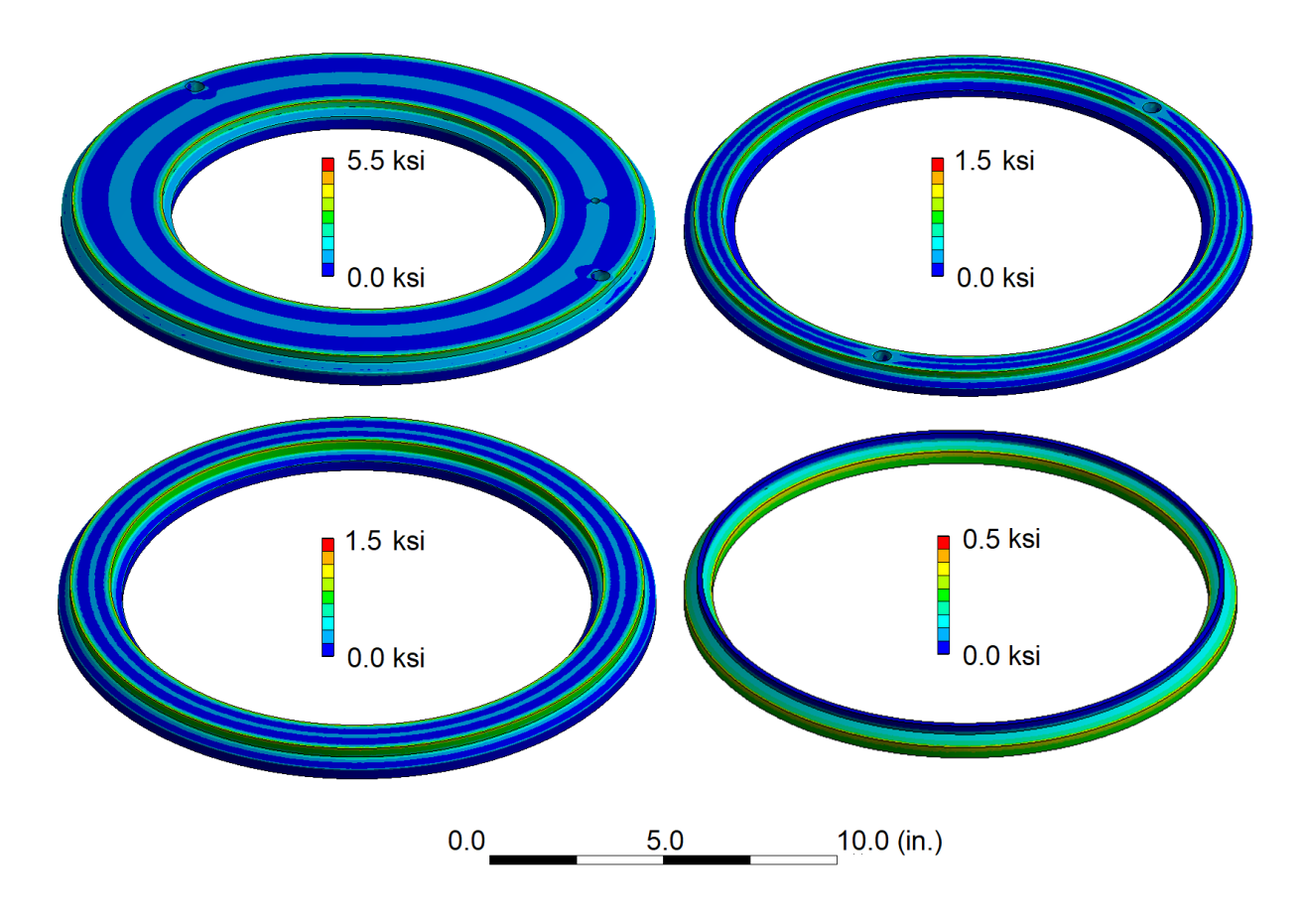


Figure A.7: Stress distribution of heat exchanger headers/rings

 Table A.7: Analysis of maximum stress results

Description	Loading	Pressure	Equivalent	Max Principal	P	S actual	S max	Pass?
Unit		psi	psi	psi	psi	psi	psi	
HX Top Ring	1	295	5856	7319	7319	7319	16700	YES
	2	17	329	290	329	329	16700	YES
HX Transition Ring	1	295	543	232	543	543	16700	YES
	2	17	31	12	31	31	16700	YES
HX 2 Ring 1	1	295	1740	1230	1740	1740	16700	YES
	2	295	1696	1121	1696	1696	16700	YES
HX 2 Ring 2	1	295	1039	452	1039	1039	16700	YES
	2	295	977	441	977	977	16700	YES
HX 2 Ring 3	1	295	1810	1628	1810	1810	16700	YES
	2	17	93	43	93	93	16700	YES
HX 1 Ring 1	1	295	1029	541	1029	1029	16700	YES
	2	295	1167	582	1167	1167	16700	YES
HX 1 Ring 2	1	295	1025	479	1025	1025	16700	YES
	2	295	961	445	961	961	16700	YES
HX 1 Ring 3	1	295	1402	795	1402	1402	16700	YES
	2	17	68	45	68	68	16700	YES
Boiler Top Plate	1	17	1676	1043	1676	1676	16700	YES
	2	85	8505	14846	14846	14846	16700	YES
Boiler Middle Plate	1	85	3574	5362	5362	5362	16700	YES
0.500" thick	2	295	12283	18058	18058	18058	16700	NO
0.625" thick		295	8806	13203	13203	13203	16700	YES

APPENDIX B: PROCESS CALCULATIONS

Table B.1: Carbon bed sizing calculations

Ru universal gas constant kJ/kmol/K 8.31 MWn2 N2 molecular weight kg/kmol 28.0 R N2 N2 gas constant kJ/kg/K 0.296 T absolute temperature K 79. PS N2 saturation pressure kPa 136. ppm parts per million contamination ppm 2 pT total pressure bar 70. pT total pressure kPa 60.012 pT total pressure kPa 0.012 pt <	Variable	Description	Unit	Value
MWn2 N2 molecular weight kg/kmol 28.0 R N2 N2 gas constant kJ/kg/K 0.296 T absolute temperature K 79. PS N2 saturation pressure kPa 136. ppm parts per million contamination ppm 2 pT total pressure bar 87.0 pT total pressure kPa 60 pD N2 partial pressure kPa 60 p N2 partial pressure kPa 0.012 log10 p torr -1.045 kPa 0.012 1.03 (eij)eq or v excess adsorbent capacity kPa 0.012 (eij)eq or v excess adsorbent capacity cal/mol 148 R Secific adsorbed N2/100 g C 1.28 necks adsorbed N2/100 g C 1.28 specific adsorbed capacity cm3 ln2/100 g C 19.3 n He mol frac He mol He/mol 0.0999 MW He He molecular weight of mix kg He/kmol				
R N2 N2 gas constant kJ/kg/K 0.296 T absolute temperature K 79. Ps N2 saturation pressure kPa 136. ppm parts per million contamination ppm 2 pT total pressure bar 2 pT total pressure kPa 60 p N2 partial pressure kPa 0.012 log10 p torr -1.045 (eij)eq or v excess adsorbent capacity kIJ/kg 221. (eij)eq or v excess adsorbent capacity cal/mol 148 N2 adsorbed N2/100 g C 1.28 specific adsorbent capacity cm3 inz/100 g C 1.28 n He mol frac He mol He/mol 0.9999 MW He He molecular weight kg He/kmol He 4.0025 n N2 mol frac N2 mol/mol 0.0000 MW N2 molecular weight of N2 kg N2/kmol N2 28.0 mass N2 per mol of mix kg N2/kmol N2 0.0005 to				
T absolute temperature				
Ps N2 saturation pressure kPa 136. ppm parts per million contamination ppm 2 pT total pressure bar 87.0 pT total pressure kPa 60 pT total pressure kPa 60 p N2 partial pressure kPa 0.012 (eij)eq or v excess adsorbent capacity kJ/kg 221. (eij)eq or v excess adsorbent capacity cal/mol 148 N2 adsorbed N2/100 g C 1.28 n N2 adsorbent capacity cm3 ln2/100g C 1.28 n He mol frac He mol He/mol 0.9999 MW He He molecular weight kg He/kmol He/mol 4.0025 n N2 mol frac N2 mol/mol 0.0000 MW N2 molecular weight of N2 kg N2/kmol N2 28.0 mass N2 per mol of mix kg N2/kmol N2 28.0 mass N2 per mol of mix kg N2/kg mix 0.0000 mol mass flow rate of He g/s 0.0000 </td <td></td> <td></td> <td></td> <td></td>				
ppm parts per million contamination ppm 2 pT total pressure psi 87.0 pT total pressure psi 87.0 pT total pressure kPa 60 p N2 partial pressure kPa 0.012 p N2 partial pressure kPa 0.012 iog10 p torr -1.045 (£ij)eq or v excess adsorbent capacity kJ/kg 221. man molification per mol of mix kg/kmol 4.025 me mol frach mol Hell mol Hell 4.002 MW Hell He molecular weight of N2 kg N2/kmol N2 4.0025 n N2 mol frac N2 mol/mol 0.0000 MW N2 molecular weight				
pT total pressure bar pT total pressure psi 87.0 pT total pressure kPa 60 p N2 partial pressure kPa 0.012 log10 p torr -1.045 (eij)eq or v excess adsorbent capacity kJ/kg 221. (eij)eq or v excess adsorbent capacity cal/mol 148 N2 adsorbed N2/100 g C 1.28 specific adsorbent capacity cal/mol 148 N2 adsorbed N2/100 g C 1.28 specific adsorbent capacity cal/mol 148 N2 adsorbed N2/100 g C 1.28 n He mol frac NE mol He/mol 0.9999 MW He He molecular weight kg He/kmol He 4.00 mass He per mol of mix kg He/kmol He 4.00 mass N2 per mol of mix kg N2/kmol N2 28.0 mass N2 per mol of mix kg N2/kmol N2 28.0 mass N2 per mol of mix kg N2/kmol N2 28.0 mot				
pT total pressure psi 87.0 pT total pressure kPa 60 p N2 partial pressure kPa 0.012 log10 p torr -1.045 (eij)eq or v excess adsorbent capacity kJ/kg 221. (eij)eq or v excess adsorbent capacity cal/mol 148 N2 adsorbed N2/100 g C 1.28 specific adsorbent capacity cm3 ln2/100g C 1.28 n He mol frac He mol He/mol 0.9999 MW He He molecular weight kg He/kmol He 4.00 mass He per mol of mix kg He/kmol 4.0025 n N2 mol frac N2 mol/mol 0.0000 MW N2 molecular weight of N2 kg N2/kmol N2 28.0 mass N2 per mol of mix kg N2/kmol N2 28.0 mass N2 per mol of mix kg N2/kmol N2 0.0005 total mass per mol of mix kg N2/kmol N2 0.0005 dof mass of N2 kg N2/kmol N2 0.0001 mdot N2 Mas				20
pT total pressure kPa 60 p N2 partial pressure kPa 0.012 log10 p torr -1.045 (εij)eq or v excess adsorbent capacity kJ/kg 221. (εij)eq or v excess adsorbent capacity kJ/kg 221. (εij)eq or v excess adsorbent capacity cal/mol 148 N2 adsorbed N2/100 g C 1.28 specific adsorbent capacity cal/mol 1.48 N2 adsorbed N2/100 g C 1.28 mas perific adsorbent capacity cm3 ln2/100 g C 1.93 n N2 mol frac He mol He/mol 0.9999 MW He He molecular weight kg He/kmol He 4.00 mass He per mol of mix kg He/kmol He 4.00 2.00 MW D mol frac N2 mol/mol 0.0000 MW N2 molecular weight of N2 kg N2/kmol N2 0.0001 MW N2 molecular weight of Mix kg N2/kmol N2 0.0001 Motal mass per mol of mix kg N2/kmol N2 0.00				6
p N2 partial pressure kPa 0.012 (εij)eq or v excess adsorbent capacity kJ/kg 221. (εij)eq or v excess adsorbent capacity cal/mol 148 N2 adsorbed N2/100 g C 1.28 specific adsorbent capacity cm3 In2/100g C 19.3 n He mol frac He mol He/mol 0.9999 MW He He molecular weight kg He/kmol He 4.00 4.0025 n N2 mol frac N2 mol/mol 0.0000 MW N2 molecular weight of N2 kg N2/kmol N2 28.0 mass N2 per mol of mix kg N2/kmol N2 0.0005 total mass per mol of mix kg N2/kmol N2 0.0005 total mass per mol of mix kg N2/kmol N2 0.0001 mdot N2 Mass flow rate of He g/s 3 mdot N2 Mass flow rate of N2 g/s 0.0041 t break through time days 22.5 N2 adsorbed g N2/tot g C 816 N2 adsorbed g N2/tot g C 816 <				
log10 p				600
(είj)eq or v excess adsorbent capacity kJ/kg 221. (είj)eq or v excess adsorbent capacity cal/mol 148 N2 adsorbed N2/100 g C 1.28 specific adsorbent capacity cm3 In2/100g C 19.3 n He mol frac He mol He/mol 0.9999 MW He He molecular weight kg He/kmol He 4.00 mass He per mol of mix kg He/kmol He 4.0025 n N2 mol frac N2 mol/mol 0.0000 MW N2 molecular weight of N2 kg N2/kmol N2 28.0 mass N2 per mol of mix kg N2/kmol N2 28.0 mass N2 per mol of mix kg N2/kmol N2 0.0005 total mass per mol of mix kg N2/kmol N2 0.0005 mod N2 mass of N2 kg N2/kmol N2 0.0001 mod N2 Mass flow rate of He g/s 3 mdot N2 Mass flow rate of N2 g/s 0.00419 t break through time days 22.5 N2 adsorbed g N2/tot g C 816 <	р		kPa	0.0120
(eij) eq or v excess adsorbent capacity cal/mol 148 N2 adsorbed N2/100 g C 1.28 specific adsorbent capacity cm3 ln2/100 g C 19.3 n He mol frac He mol He/mol 0.9999 MW He He molecular weight kg He/kmol He 4.0025 n N2 mol frac N2 mol/mol 0.0000 MW N2 molecular weight of N2 kg N2/kmol N2 28.0 mass N2 per mol of mix kg N2/kmol N2 0.0005 total mass per mol of mix kg N2/kmol N2 0.0005 total mass per mol of mix kg N2/kg mix 0.0001 mdot He Mass flow rate of He g/s 0.00419 t break through time days 22.5 N2 adsorbed g N2/tot g C 816 N2 adsorbed N2 adsorbed g N2/tot g C 816 N2 adsorption capacity cm3 ln2/ 100 g C 19.3 rho N2 density of N2 at T kg/m3 793. m c mass of carbon kg 53.3				
N2 adsorbed N2/100 g C 1.28	(ɛij)eq or v			221.2
specific adsorbent capacity cm3 In2/100g C 19.3 n He mol frac He mol He/mol 0.9999 MW He He molecular weight kg He/kmol 4.0025 n N2 mol frac N2 mol/mol 0.0000 MW N2 molecular weight of N2 kg N2/kmol N2 28.0 mass N2 per mol of mix kg N2/kmol N2 0.0005 total mass per mol of mix kg/kmol 4.0030 % of mass of N2 kg N2/kg mix 0.0001 mdot He Mass flow rate of He g/s 3 mdot N2 Mass flow rate of N2 g/s 0.00419 t break through time days 22.5 N2 adsorbed g N2/tot g C 816 N2 adsorbed g N2/tot g C 816 N2 adsorption capacity cm3 In2/ 100 g C 19.3 rho N2 density of N2 at T kg/m3 793. m c mass of carbon kg kg/m3 3.3 p c density of carbon kg 4.9 L	(ɛij)eq or v			1481
n He mol frac He mol He/mol 0.9999 MW He He molecular weight kg He/kmol He 4.0025 n N2 mol frac N2 mol/mol 0.0000 MW N2 molecular weight of N2 kg N2/kmol N2 28.0 mass N2 per mol of mix kg N2/kmol N2 0.0005 total mass per mol of mix kg/kmol 4.0030 % of mass of N2 kg N2/kg mix 0.0001 mdot He Mass flow rate of He g/s 3 mdot N2 Mass flow rate of N2 g/s 0.00419 t break through time days 22.5 N2 adsorbed g N2/tot g C 816 N2 adsorbed g N2/tot g C 816 N2 adsorbed of N2 adsorbed g N2/tot g C 816 N2 adsorbed of N2 adsorbed of N2 adsorbed of Carbon of N2 adsorbed of Carbon of N2 kg/m3 793.3 m c mass of carbon of Raman of Carbon o				1.286
MW He He molecular weight mass He per mol of mix kg He/kmol 4.0025 n N2 mol frac N2 mol/mol 0.0000 MW N2 molecular weight of N2 kg N2/kmol N2 28.0 mass N2 per mol of mix kg N2/kmol N2 0.0005 total mass per mol of mix kg/kmol 4.0030 % of mass of N2 kg N2/kg mix 0.0001 mdot He Mass flow rate of He g/s 0.00419 t break through time days 22.5 N2 adsorbed g N2/tot g C 816 N2 adsorbed g N2/tot g C		specific adsorbent capacity	cm3 In2/100g C	19.30
n N2 mol frac N2 mol/mol 0.0000 MW N2 molecular weight of N2 kg N2/kmol N2 28.0 mass N2 per mol of mix kg N2/kmol N2 0.0005 total mass per mol of mix kg/kmol 4.0030 % of mass of N2 kg N2/kg mix 0.0001 mdot He Mass flow rate of He g/s 3 mdot N2 Mass flow rate of N2 g/s 0.00419 t break through time days 22.5 N2 adsorbed g N2/tot g C 816 N2 adsorbed N2 adsorbed g N2/tot g C 816 N2 adsorbed N2 adsorbed g N2/tot g C 816 N2 adsorbed N2 adsorbed g N2/tot g C 816 N2 adsorbed N2 adsorbed g N2/tot g C 816 N2 adsorbed N2 adsorbed g N2/tot g C 816 N2 adsorbed N2 adsorbed g N2/tot g C 816 N2 adsorbed N2 adsorbed g N2/tot g C 816 N2 adsorbed N2 adsorbed g N2/tot g C 816 N2 adsorbed N2 adsorbed g N2/tot g C 816	n He		mol He/mol	0.99998
n N2 mol frac N2 mol/mol 0.0000 MW N2 molecular weight of N2 kg N2/kmol N2 28.0 mass N2 per mol of mix kg N2/kmol N2 0.0005 total mass per mol of mix kg N2/kg mix 0.0001 modot He Mass flow rate of He g/s 3 mdot N2 Mass flow rate of N2 g/s 0.00419 t break through time days 22.5 N2 adsorbed g N2/tot g C 816 N2 adsorbed g N2/tot g C 816 N2 adsorbed N2 adsorbed g N2/tot g C 816 N2 adsorbed 9 N2/tot g C 816 N2 adsorbed N2 adsorbed g N2/tot g C 816 N2/tot g C 816 N2 adsorbed N2 adsorbed g N2/tot g C 816 N2/tot g C 816 N2 adsorbed N2 adsorbed g N2/tot g C 816 N2/tot g C 816 N2 adsorbed N2 adsorbed g N2/tot g C 816 92/tot g C 816 N2 adsorbed N2 adsorbed g N2/tot g C <td>MW He</td> <td>He molecular weight</td> <td>kg He/kmol He</td> <td>4.003</td>	MW He	He molecular weight	kg He/kmol He	4.003
MW N2 molecular weight of N2 kg N2/kmol N2 28.0 mass N2 per mol of mix kg N2/kmol N2 0.0005 total mass per mol of mix kg N2/kmol N2 0.0001 % of mass of N2 kg N2/kg mix 0.0001 mdot He Mass flow rate of He g/s 3 mdot N2 Mass flow rate of N2 g/s 0.00419 t break through time days 22.5 N2 adsorbed g N2/tot g C 816 N2 adsorbed g N2/tot g C 816 N2 adsorption capacity cm3 In2/ 100 g C 19.3 rho N2 density of N2 at T kg/m3 793. m c mass of carbon kg 53.3 p c density of carbon g/cm3 0.4 V c volume of carbon in3 739 R bed length/diameter 4.9 4.9 L bed length in 61.3 D bed diameter in 12.3 R He He gas constant kJ/kg/		mass He per mol of mix	kg He/kmol	4.00252
mass N2 per mol of mix kg N2/kmol N2 0.0005 total mass per mol of mix kg/kmol 4.0030 % of mass of N2 kg N2/kg mix 0.0001 mdot He Mass flow rate of He g/s 3 mdot N2 Mass flow rate of N2 g/s 0.00419 t break through time days 22.5 N2 adsorbed g N2/tot g C 816 N2 adsorbed g N2/tot g C 816 N2 adsorbed g N2/tot g C 816 N2 adsorption capacity cm3 In2/ 100 g C 19.3 rho N2 density of N2 at T kg/m3 793. m c mass of carbon kg 53.3 p c density of carbon g/cm3 0.4 V c volume of carbon in3 739 R bed length/diameter 4.9 L bed length in 61.3 D bed diameter in 12.3 R He He gas constant kJ/kg/K 2.07 rho	n N2	mol frac N2	mol/mol	0.00002
total mass per mol of mix kg/kmol 4.0030 % of mass of N2 kg N2/kg mix 0.0001 mdot He Mass flow rate of He g/s 3 mdot N2 Mass flow rate of N2 g/s 0.00419 t break through time days 22.5 N2 adsorbed N2 adsorbed g N2/tot g C 816 N2 adsorption capacity cm3 ln2/ 100 g C 19.3 rho N2 density of N2 at T kg/m3 793. m c mass of carbon kg 53.3 p c density of carbon g/cm3 0.4 V c volume of carbon in3 739 R bed length/diameter 4.9 L bed length in 61.3 D bed diameter in 12.3 R He He gas constant kJ/kg/K 2.07 rho He rho of He at process conditions kg/m3 3.62 A cross-sectional area of bed in2 120. μ visocity Pa*s 0.000018 Dp particle diameter mm rho b kg/m3 50 rho p kg/m3 77 ε emmisivity of carbon 0.356 Q volumetric flow rate m3/s 0.008 A flow area m2 0.077 vs flow velocity m/s 0.106	MW N2	molecular weight of N2	kg N2/kmol N2	28.01
% of mass of N2 kg N2/kg mix 0.0001 mdot He Mass flow rate of He g/s 3 mdot N2 Mass flow rate of N2 g/s 0.00419 t break through time days 22.5 N2 adsorbed g N2/tot g C 816 N2 adsorption capacity cm3 In2/100 g C 19.3 rho N2 density of N2 at T kg/m3 793. m c mass of carbon kg 53.3 p c density of carbon g/cm3 0.4 V c volume of carbon in3 739 R bed length/diameter 4.9 L bed length in 61.3 D bed diameter in 12.3 R He He gas constant kJ/kg/K 2.07 rho He rho of He at process conditions kg/m3 3.62 A cross-sectional area of bed in2 120. µ visocity Pa*s 0.000018 Dp particle diameter <		mass N2 per mol of mix	kg N2/kmol N2	0.00056
mdot He Mass flow rate of He g/s 3 mdot N2 Mass flow rate of N2 g/s 0.00419 t break through time days 22.5 N2 adsorbed g N2/tot g C 816 N2 adsorption capacity cm3 In2/100 g C 19.3 rho N2 density of N2 at T kg/m3 793. m c mass of carbon kg 53.3 ρ c density of carbon g/cm3 0.4 V c volume of carbon in3 739 R bed length/diameter 4.9 L bed length in 61.3 D bed diameter in 12.3 R He He gas constant kJ/kg/K 2.07 rho He rho of He at process conditions kg/m3 3.62 A cross-sectional area of bed in2 120. µ visocity Pa*s 0.000018 Dp particle diameter mm rho b kg/m3 77		total mass per mol of mix	kg/kmol	4.00308
mdot N2 Mass flow rate of N2 g/s 0.00419 t break through time days 22.5 N2 adsorbed g N2/tot g C 816 N2 adsorption capacity cm3 In2/100 g C 19.3 rho N2 density of N2 at T kg/m3 793. m c mass of carbon kg 53.3 p c density of carbon g/cm3 0.4 V c volume of carbon in3 739 R bed length/diameter 4.9 4.9 L bed length in 61.3 D bed diameter in 12.3 R He He gas constant kJ/kg/K 2.07 rho He rho of He at process conditions kg/m3 3.62 A cross-sectional area of bed in2 120. µ visocity Pa*s 0.000018 Dp particle diameter mm rho b kg/m3 50 rho p kg/m3 77		% of mass of N2	kg N2/kg mix	0.00014
t break through time days 22.5 N2 adsorbed N2 adsorbed g N2/tot g C 816 N2 adsorption capacity cm3 In2/100 g C 19.3 rho N2 density of N2 at T kg/m3 793. m c mass of carbon kg 53.3 ρ c density of carbon g/cm3 0.4 V c volume of carbon in3 739 R bed length/diameter 4.9 L bed length in 61.3 D bed diameter in 12.3 R He He gas constant kJ/kg/K 2.07 rho He rho of He at process conditions kg/m3 3.62 A cross-sectional area of bed in2 120. μ visocity Pa*s 0.000018 Tho b kg/m3 50 rho p kg/m3 77 ε emmisivity of carbon 0.356 Q volumetric flow rate m3/s 0.008 A flow area m2 0.077 γs flow velocity m/s 0.106	mdot He	Mass flow rate of He	g/s	30
N2 adsorbed N2 adsorption capacity cm3 In2/ 100 g C 19.3 rho N2 density of N2 at T kg/m3 793. m c mass of carbon kg 53.3 ρ c density of carbon g/cm3 0.4 V c volume of carbon in3 739 R bed length/diameter 4.9 L bed length in 61.3 D bed diameter in 12.3 R He He gas constant kJ/kg/K 2.07 rho He rho of He at process conditions kg/m3 3.62 A cross-sectional area of bed in2 120. µ visocity Pa*s 0.000018 Dp particle diameter mm rho b kg/m3 50 rho p kg/m3 77 ε emmisivity of carbon 0.356 Q volumetric flow rate m3/s 0.008 A flow area m2 0.077 vs<	mdot N2	Mass flow rate of N2	g/s	0.004199
N2 adsorption capacity	t	break through time	days	22.52
rho N2 density of N2 at T kg/m3 793. m c mass of carbon kg 53.3 ρ c density of carbon g/cm3 0.4 V c volume of carbon in3 739 R bed length/diameter 4.9 L bed length in 61.3 D bed diameter in 12.3 R He He gas constant kJ/kg/K 2.07 rho He rho of He at process conditions kg/m3 3.62 A cross-sectional area of bed in2 120. μ visocity Pa*s 0.000018 Dp particle diameter mm rho b kg/m3 50 rho p kg/m3 77 ε emmisivity of carbon 0.356 Q volumetric flow rate m3/s 0.008 A flow area m2 0.077 vs flow velocity m/s 0.106	N2 adsorbed	N2 adsorbed	g N2/tot g C	8169
m c mass of carbon kg 53.3 ρ c density of carbon g/cm3 0.4 V c volume of carbon in3 739 R bed length/diameter 4.9 L bed length in 61.3 D bed diameter in 12.3 R He He gas constant kJ/kg/K 2.07 rho He rho of He at process conditions kg/m3 3.62 A cross-sectional area of bed in2 120. μ visocity Pa*s 0.000018 Dp particle diameter mm rho b kg/m3 50 rho p kg/m3 50 rho p kg/m3 77 ε emmissivity of carbon 0.356 Q volumetric flow rate m3/s 0.008 A flow area m2 0.077 vs flow velocity m/s 0.106		N2 adsorption capacity	cm3 In2/ 100 g C	19.30
ρ c density of carbon g/cm3 0.4 V c volume of carbon in3 739 R bed length/diameter 4.9 L bed length in 61.3 D bed diameter in 12.3 R He He gas constant kJ/kg/K 2.07 rho He rho of He at process conditions kg/m3 3.62 A cross-sectional area of bed in2 120 μ visocity Pa*s 0.000018 Dp particle diameter mm rho b kg/m3 50 rho p kg/m3 77 ε emmisivity of carbon 0.356 Q volumetric flow rate m3/s 0.008 A flow area m2 0.077 vs flow velocity m/s 0.106	rho N2	density of N2 at T	kg/m3	793.9
V c volume of carbon in3 739 R bed length/diameter 4.9 L bed length in 61.3 D bed diameter in 12.3 R He He gas constant kJ/kg/K 2.07 rho He rho of He at process conditions kg/m3 3.62 A cross-sectional area of bed in2 120. μ visocity Pa*s 0.000018 Dp particle diameter mm rho b kg/m3 50 rho p kg/m3 77 ε emmisivity of carbon 0.356 Q volumetric flow rate m3/s 0.008 A flow area m2 0.077 vs flow velocity m/s 0.106	m c	mass of carbon	kg	53.30
R bed length/diameter 4.9 L bed length in 61.3 D bed diameter in 12.3 R He He gas constant kJ/kg/K 2.07 rho He rho of He at process conditions kg/m3 3.62 A cross-sectional area of bed in2 120. μ visocity Pa*s 0.000018 Dp particle diameter mm rho b kg/m3 50 rho p kg/m3 77 ε emmisivity of carbon 0.356 Q volumetric flow rate m3/s 0.008 A flow area m2 0.077 vs flow velocity m/s 0.106	рс	density of carbon	g/cm3	0.44
L bed length in 61.3 D bed diameter in 12.3 R He He gas constant kJ/kg/K 2.07 rho He rho of He at process conditions kg/m3 3.62 A cross-sectional area of bed in2 120. μ visocity Pa*s 0.000018 Dp particle diameter mm 50 rho b kg/m3 50 rho p kg/m3 77 ε emmissivity of carbon 0.356 Q volumetric flow rate m3/s 0.008 A flow area m2 0.077 vs flow velocity m/s 0.106	V c	volume of carbon	in3	7392
D bed diameter in 12.3 R He He gas constant kJ/kg/K 2.07 rho He rho of He at process conditions kg/m3 3.62 A cross-sectional area of bed in2 120. μ visocity Pa*s 0.000018 Dp particle diameter mm 50 rho b kg/m3 77 ε emmisivity of carbon 0.356 Q volumetric flow rate m3/s 0.008 A flow area m2 0.077 vs flow velocity m/s 0.106	R	bed length/diameter		4.95
D bed diameter in 12.3 R He He gas constant kJ/kg/K 2.07 rho He rho of He at process conditions kg/m3 3.62 A cross-sectional area of bed in2 120. μ visocity Pa*s 0.000018 Dp particle diameter mm rho b kg/m3 50 rho p kg/m3 77 ε emmissivity of carbon 0.356 Q volumetric flow rate m3/s 0.008 A flow area m2 0.077 vs flow velocity m/s 0.106	L	bed length	in	61.31
rho He rho of He at process conditions kg/m3 3.62 A cross-sectional area of bed in2 120. μ visocity Pa*s 0.000018 Dp particle diameter mm rho b kg/m3 50 rho p kg/m3 77 ε emmissivity of carbon 0.356 Q volumetric flow rate m3/s 0.008 A flow area m2 0.077 vs flow velocity m/s 0.106	D		in	12.39
rho He rho of He at process conditions kg/m3 3.62 A cross-sectional area of bed in2 120. μ visocity Pa*s 0.000018 Dp particle diameter mm rho b kg/m3 50 rho p kg/m3 77 ε emmissivity of carbon 0.356 Q volumetric flow rate m3/s 0.008 A flow area m2 0.077 vs flow velocity m/s 0.106	R He	He gas constant	kJ/kg/K	2.077
A cross-sectional area of bed in2 120. μ visocity Pa*s 0.000018 Dp particle diameter mm rho b kg/m3 50 rho p kg/m3 77 ε emmisivity of carbon 0.356 Q volumetric flow rate m3/s 0.008 A flow area m2 0.077 vs flow velocity m/s 0.106	rho He			3.620
μ visocity Pa*s 0.000018 Dp particle diameter mm rho b kg/m3 50 rho p kg/m3 77 ε emmissivity of carbon 0.356 Q volumetric flow rate m3/s 0.008 A flow area m2 0.077 vs flow velocity m/s 0.106	Α			120.6
Dp particle diameter mm rho b kg/m3 50 rho p kg/m3 77 ε emmisivity of carbon 0.356 Q volumetric flow rate m3/s 0.008 A flow area m2 0.077 vs flow velocity m/s 0.106		visocity	Pa*s	0.0000187
rho b kg/m3 50 rho p kg/m3 77 ε emmisivity of carbon 0.356 Q volumetric flow rate m3/s 0.008 A flow area m2 0.077 vs flow velocity m/s 0.106			mm	5
rho p kg/m3 77 ε emmisivity of carbon 0.356 Q volumetric flow rate m3/s 0.008 A flow area m2 0.077 vs flow velocity m/s 0.106				500
ε emmisivity of carbon 0.356 Q volumetric flow rate m3/s 0.008 A flow area m2 0.077 vs flow velocity m/s 0.106				777
Q volumetric flow rate m3/s 0.008 A flow area m2 0.077 vs flow velocity m/s 0.106		emmisivity of carbon		0.3565
A flow area m2 0.077 vs flow velocity m/s 0.106	Q		m3/s	0.0083
vs flow velocity m/s 0.106	A			0.0778
				0.1065
IAF IDTESSUTE GTOD IDSI I 0.0708	ΔΡ	pressure drop	psi	0.0708

APPENDIX C: MECHANICAL CALCULATIONS

Table C.1: B31.3 piping pressure design

Variable	Description	Unit	2 NPS	1 NPS	1/2 NPS	1/2" OD	1/2" OD Cu	3 NPS	1 NPS	1/2 NPS
	fluid in pipe		Helium	Helium	Helium	Helium	Helium	Nitrogen	Nitrogen	Nitrogen
P	design pressure	psi	295	295	295	295	295	85	85	85
D (do)	outer diameter	in	2.375	1.315	0.84	0.5	0.5	3.5	1.315	0.84
S	allowable stress	psi	16700	16700	16700	16700	3380	16700	16700	16700
E	weld factor		0.65	0.65	0.65	0.65	0.65	0.65	0.65	0.65
W	weld joint strength reduction factor		1	1	1	1	1	1	1	1
Y	material/temperature coefficient		0.4	0.4	0.4	0.4	0.4	0.4	0.4	0.4
tm	internmediate thickness	in	0.0319	0.0177	0.0113	0.0067	0.0319	0.0137	0.0051	0.0033
tol	maximum tolerance	%	12.5	12.5	12.5	12.5	12.5	12.5	12.5	12.5
t design	design thickness	in	0.0365	0.0202	0.0129	0.0077	0.0364	0.0156	0.0059	0.0037
t actual	Actual thickness of pipe	in	0.1090	0.1090	0.0830	0.0490	0.0490	0.1200	0.1090	0.0830

Table C.2: BPVC internal pressure design

Variable	Description	HX-2 Mandrel	HX-2 Shell	HX-1 Mandrel	HX-1 Shell	N2 Boiler	Carbon Bed	CB N2 Tank
P	design pressure	17	265	17	265	160	265	160
Do	outside diameter	10.75	13.077	14.2	17.25	6.625	12.75	3.5
t	thickness	0.3650	0.1875	0.1875	0.1875	0.1340	0.1800	0.1200
R	inside radius	5.010	6.351	6.913	8.438	3.179	6.195	1.630
S	allowable stress	20000	20000	20000	20000	20000	20000	20000
E	quality factor	0.65	0.65	0.65	0.65	1	0.65	0.65
t design	required thickness	0.0066	0.1311	0.0090	0.1741	0.0256	0.1278	0.0202
P design	pressure capability	907.4	377.1	347.0	285.1	822.4	371.3	916.6

 Table C.3: BPVC external pressure design

Variable	Description	Unit	HX-2 Mandrel	HX-2 Shell	HX-1 Mandrel	HX-1 Shell
P	required pressure	psi	265	17	265	17
Do	outer diameter	in	10.75	13.13	14.20	16.58
t	thickness	in	0.3650	0.1875	0.1875	0.1875
L	length	in	88	84	80	78
Le	effective length	in	17.60	84.00	13.33	78.00
Do/t	diameter to thickness ratio		29.45	70.00	75.73	88.40
L/Do	length to diameter ratio		1.64	6.40	0.94	4.71
A	factor		0.0016	0.00033	0.0023	0.00031
Е	modulus of elasticity	psi	28000000	28000000	28000000	28000000
В	factor		10800	4600	11900	4350
Pa	design pressure	psi	488.9	87.6	209.5	65.6

Table C.4: HX-1 mandrel vertical rod supports

Variable	Description	Unit	Value
Do	outer diameter	in	14.2
t	thickness	in	0.1875
r	outer radius	in	7.1
n	number of supports		4
r/t			37.87
requirement			10
pass?	intermediate test		YES
L	length	in	80
requirement			214.1
pass?	intermediate test		YES
E	modulus of elasticity	psi	28000000
ν	poisson's ratio		0.3
βcr	capacity reduction factor		0.8
nSF	safety factor from BPVC		2.5
q'1	conditional q'	psi	103.6
q'2	conditional q'	psi	305.6
q'	critical pressure	psi	305.6

 Table C.5: Reinforced nozzle opening in carbon bed top head

Variable	Description	Unit	Value
A	required area	in2	0.30364
d	inside opening diameter	in	2.375
tr	required thickness	in	0.12785
F	correction factor		1
tn	nozzle wall thickness	in	0.109
fr1	Sn/Sv for nozzle wall		1
Sn	allowable stress in nozzle	psi	20000
Sv	allowable stress in vessel	psi	20000
A1	available area per section	in2	0.07043
E1	weld factor		1
t	specified vessel wall thickness	in	0.1575
A2	available area in nozzle	in2	0.05155
trn	required thickness for seamless nozzle wall	in	0.0144
fr2	Sn/Sv for vessel wall		1
Sum	available area	in2	0.12198
Pass?	If pass, no need for sleeve		NO
Ar	required extra area	in2	0.18165
Ls	sleeve length	in	1.5
ts	required sleeve thickness	in	0.1211
ts_actual	actual sleeve thickness	in	0.125
ID	inside diameter of sleeve	in	2.375
OD	outside diameter of sleeve	in	2.625

Table C.6: Carbon bed screen supports

Variable	Description	Unit	Value
b	horizontal width of beam	in	0.25
d	vertical depth of beam	in	0.75
E	modulus of elasticity	psi	28000000
G	shear modulus	psi	11200000
I	length on beam	in	11.54
а	half the vertical depth of beam	in	0.375
Ρ'	specifically distributed critical load	lbs	3514
W'	uniformly distributed critical load	lbs	5868
Ρ'	critical load at centroid	lbs	6137
dPmax	max pressure difference	psi	29
Α	area from which it is held	in2	2.885
Pdp	max load from pressure difference	lbs	83.66
ms	screen mass	lbs	42.24
Α	area from which it is held	in2	2.885
Ps	screen pressure	psi	14.64
Pass?	test		YES

 Table C.7: Component weight

Component	Material	Weight (lbs)	Total (lbs)	
Heat Exchanger	Steel	876.3	1129.9	
Tieat Excilatige	Copper	253.6	1123.3	
Nitrogen Boiler	Steel	134.8	204.3	
Mitrogen Boner	LN2	LN2 69.5		
	Steel	371.1		
Carbon Bed	Carbon	400.1	788.7	
	LN2	17.5		
Purifier	·		2122.9	

Table C.8: Component cool-down enthalpy

Component	Material	Weight (lbs)	ΔH (kJ/kg)	Cool-Down Enthalpy (kJ)
Heat Exchanger	Steel	876.3	82.84	32928
neat excitatiget	Copper	253.6	73.56	8462
Nitrogen Boiler	Steel	134.8	82.84	5065
Carbon Bed	Steel	371.1	82.84	13945
Carbon Bed	Carbon	400.1	276.3	50148

BIBLIOGRAPHY

BIBLIOGRAPHY

- [1] Hamak J E 2015 Minerals Handbook. United States Geological Survey) p 9
- [2] Casagrande F, Campisi I, Gurd P, Hatfield D, Howell M, Stout D, Strong H, Arenius D, Creel J, Dixon K, Ganni V and Knudsen P 2005 Status of the Cryogenic System Commissioning at SNS. In: *Proceedings of the 2005 Particle Accelerator Conference*, pp 970-2
- [3] Thomas E R and Denton R D 1988 Conceptual studies for CO2/natural gas separation using the controlled freeze zone (CFZ) process *Gas Separation & Purification* 2 84 9
- [4] Dauvergne J P, Delikaris D, Haug F and Knoops S 1994 A helium freeze-out cleaner operating at atmospheric pressure *Cryogenics* 34 135 8
- [5] Scholes C A and Ghosh U K 2017 Review of Membranes for Helium Separation and Purification *Membranes* 7 9
- [6] Personal Conversation with V. Ganni, Director for MSU Cryogenics Initiative
- [7] Yuksek E 2009 Capacity Improvement of a Small-Scale Cryogenic System Using Exergy Analysis. In: *Mechanical Engineering*: Old Dominion University) p 79
- [8] Flatau P J, Walko R L and Cotton W R 1992 Polynomial Fits to Saturation Vapor Pressure Journal of Applied Meteorology 31 1507-13
- [9] Wright M 2009 Design and Development of a Helium Purifier. In: *Mechanical Engineering*, (Virginia, USA: Old Dominion University) p 87
- [10] Young, Warren C, and Richard G Budynas. *Roark's Formulas for Stress and Strain*. 7th ed., McGraw-Hill, 2002.
- [11] Personal Conversation with M. Wright, Cryogenic Engineer, FRIB